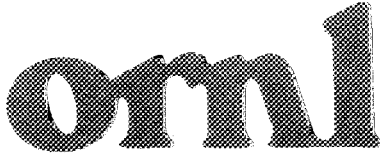




3 4456 0289962 9

ORNL/TM-11038



OAK RIDGE  
NATIONAL  
LABORATORY



**Shield Optimization Program, Part VI:  
The Effect of Impurity Layers on the  
Hydrodynamic Response of a Beryllium  
Target to Mono-Energetic X-Rays  
Using the PUFF-TFT Code**

M. S. Smith  
S. McNeany  
R. T. Santoro  
T. A. Gabriel

OAK RIDGE NATIONAL LABORATORY  
CENTRAL RESEARCH LIBRARY  
CIRCULATION SECTION  
OAK RIDGE, TN  
**LIBRARY LOAN COPY**  
DO NOT TRANSFER TO ANOTHER PERSON  
If you wish someone else to see this  
report, send in name with report and  
the library will arrange a loan.

OPERATED BY  
MARTIN MARIETTA ENERGY SYSTEMS, INC.  
FOR THE UNITED STATES  
DEPARTMENT OF ENERGY

Prepared in the United States of America. Available from  
National Technical Information Service  
U.S. Department of Commerce  
5285 Port Royal Road, Springfield, Virginia 22161  
NTIS price codes--Printed Copy (A05) Microfilm (A01)

This report was prepared as an account of work sponsored by an agency of the United States Government. Neither the United States Government nor any agency thereof, nor any of their employees, makes any warranty, express or implied, or assumes any legal liability or responsibility for the accuracy, completeness, or usefulness of any information, apparatus, product, or process disclosed, or represents that its use would not infringe privately owned rights. Reference herein to any specific commercial product, process, or service by trade name, trademark, manufacturer, or otherwise, does not necessarily constitute or imply its endorsement, recommendation, or favoring by the United States Government or any agency thereof. The views and opinions of authors expressed herein do not necessarily state or reflect those of the United States Government or any agency thereof.

ORNL/TM-11038

Engineering Physics and Mathematics Division

**Shield Optimization Program, Part VI:  
The Effect of Impurity Layers on the  
Hydrodynamic Response of a Beryllium Target to  
Mono-Energetic X-Rays Using the PUFF-TFT Code**

M. S. Smith, S. McNeany,\* R. T. Santoro, and T. A. Gabriel

DATE PUBLISHED — March 1989

\*Engineering Technology Division

Prepared by the  
OAK RIDGE NATIONAL LABORATORY  
Oak Ridge, Tennessee 37831  
operated by  
MARTIN MARIETTA ENERGY SYSTEMS, INC.  
for the  
U.S. DEPARTMENT OF ENERGY  
under contract DE-AC05-84OR21400



3 4456 0289962 9



## CONTENTS

ABSTRACT . . . . .	xi
1. INTRODUCTION . . . . .	1
2. METHODOLOGY . . . . .	3
3. RESULTS AND DISCUSSION . . . . .	5
3.1 SOURCE TERM NO. 1: 1 keV, 1 cal/cm <sup>2</sup> . . . . .	5
3.2 SOURCE TERM NO. 2: 1 keV, 5 cal/cm <sup>2</sup> . . . . .	6
3.3 SOURCE TERM NO. 3: 2 keV, 1 cal/cm <sup>2</sup> . . . . .	6
3.4 SOURCE TERM NO. 4: 2 keV, 5 cal/cm <sup>2</sup> . . . . .	7
4. CONCLUSIONS . . . . .	8
APPENDIX A . . . . .	57
REFERENCES . . . . .	58



## LIST OF FIGURES

<u>Figure</u>		<u>Page</u>
1	Energy deposited as a function of depth for the 1 keV, 1 cal/cm <sup>2</sup> source incident upon the beryllium substrate (no surface impurity layer) .	9
2	Energy deposited as a function of depth for the 1 keV, 1 cal/cm <sup>2</sup> source incident upon the 300Å thick surface impurity layer with the base impurity concentrations . . . . .	10
3	Energy deposited as a function of depth for the 1 keV, 1 cal/cm <sup>2</sup> source incident upon the 300Å thick surface impurity layer with triple impurity concentrations . . . . .	11
4	Axial stress as a function of depth at 0.5 nanosecond for the 1 keV, 1 cal/cm <sup>2</sup> source incident upon the beryllium substrate (no surface impurity layer) . . . . .	12
5	Lateral stress as a function of depth at 0.5 nanosecond for the 1 keV, 1 cal/cm <sup>2</sup> source incident upon the beryllium substrate (no surface impurity layer) . . . . .	13
6	Axial stress as a function of depth at 0.5 nanosecond for the 1 keV, 1 cal/cm <sup>2</sup> source incident upon the 300Å thick surface impurity layer with the base impurity concentrations . . . . .	14
7	Lateral stress as a function of depth at 0.5 nanosecond for the 1 keV, 1 cal/cm <sup>2</sup> source incident upon the 300Å thick surface impurity layer with the base impurity concentrations . . . . .	15
8	Axial stress as a function of depth at 0.5 nanosecond for the 1 keV, 1 cal/cm <sup>2</sup> source incident upon the 300Å thick surface impurity layer with triple impurity concentrations . . . . .	16
9	Lateral stress as a function of depth at 0.5 nanosecond for the 1 keV, 1 cal/cm <sup>2</sup> source incident upon the 300Å thick surface impurity layer with triple impurity concentrations . . . . .	17
10	Temperature as a function of depth at specific times for the 1 keV, 5 cal/cm <sup>2</sup> source incident upon the beryllium substrate (no surface impurity layer) . . . . .	18
11	Temperature as a function of depth at specific times for the 1 keV, 5 cal/cm <sup>2</sup> source incident upon the 300Å thick surface impurity layer with the base impurity concentrations . . . . .	19

<u>Figure</u>	<u>Page</u>
12	Temperature as a function of depth at specific times for the 1 keV, 5 cal/cm <sup>2</sup> source incident upon the 300Å thick surface impurity layer with triple impurity concentrations . . . . . 20
13	Energy deposited as a function of depth for the 1 keV, 5 cal/cm <sup>2</sup> source incident upon the beryllium substrate (no surface impurity layer) . . . . . 21
14	Energy deposited as a function of depth for the 1 keV, 5 cal/cm <sup>2</sup> source incident upon the 300Å thick surface impurity layer with the base impurity concentrations . . . . . 22
15	Energy deposited as a function of depth for the 1 keV, 5 cal/cm <sup>2</sup> source incident upon the 300Å thick surface impurity layer with triple impurity concentrations . . . . . 23
16	Axial stress as a function of depth at 1.0 nanosecond for the 1 keV, 5 cal/cm <sup>2</sup> source incident upon the beryllium substrate (no surface impurity layer) . . . . . 24
17	Lateral stress as a function of depth at 1.0 nanosecond for the 1 keV, 5 cal/cm <sup>2</sup> source incident upon the beryllium substrate (no surface impurity layer) . . . . . 25
18	Axial stress as a function of depth at 1.0 nanosecond for the 1 keV, 5 cal/cm <sup>2</sup> source incident upon the 300Å thick surface impurity layer with the base impurity concentrations . . . . . 26
19	Lateral stress as a function of depth at 1.0 nanosecond for the 1 keV, 5 cal/cm <sup>2</sup> source incident upon the 300Å thick surface impurity layer with the base impurity concentrations . . . . . 27
20	Axial stress as a function of depth at 1.0 nanosecond for the 1 keV, 5 cal/cm <sup>2</sup> source incident upon the 300Å thick surface impurity layer with triple impurity concentrations . . . . . 28
21	Lateral stress as a function of depth at 1.0 nanosecond for the 1 keV, 5 cal/cm <sup>2</sup> source incident upon the 300Å thick surface impurity layer with triple impurity concentrations . . . . . 29
22	Temperature as a function of depth at specific times for the 1 keV, 5 cal/cm <sup>2</sup> source incident upon the beryllium substrate (no surface impurity layer) . . . . . 30
23	Temperature as a function of depth at specific times for the 1 keV, 5 cal/cm <sup>2</sup> source incident upon the 300Å thick surface impurity layer with the base impurity concentrations . . . . . 31

<u>Figure</u>	<u>Page</u>
24	Temperature as a function of depth at specific times for the 1 keV, 5 cal/cm <sup>2</sup> source incident upon the 300Å thick surface impurity layer with triple impurity concentrations . . . . . 32
25	Energy deposited as a function of depth for the 2 keV, 1 cal/cm <sup>2</sup> source incident upon the beryllium substrate (no surface impurity layer) . . . . . 33
26	Energy deposited as a function of depth for the 2 keV, 1 cal/cm <sup>2</sup> source incident upon the 300Å thick surface impurity layer with the base impurity concentrations . . . . . 34
27	Energy deposited as a function of depth for the 2 keV, 1 cal/cm <sup>2</sup> source incident upon the 300Å thick surface impurity layer with triple impurity concentrations . . . . . 35
28	Axial stress as a function of depth at 3.0 nanoseconds for the 2 keV, 1 cal/cm <sup>2</sup> source incident upon the beryllium substrate (no surface impurity layer) . . . . . 36
29	Lateral stress as a function of depth at 3.0 nanoseconds for the 2 keV, 1 cal/cm <sup>2</sup> source incident upon the beryllium substrate (no surface impurity layer) . . . . . 37
30	Axial stress as a function of depth at 3.0 nanoseconds for the 2 keV, 1 cal/cm <sup>2</sup> source incident upon the 300Å thick surface impurity layer with the base impurity concentrations . . . . . 38
31	Lateral stress as a function of depth at 3.0 nanoseconds for the 2 keV, 1 cal/cm <sup>2</sup> source incident upon the 300Å thick surface impurity layer with the base impurity concentrations . . . . . 39
32	Axial stress as a function of depth at 3.0 nanoseconds for the 2 keV, 1 cal/cm <sup>2</sup> source incident upon the 300Å thick surface impurity layer with triple impurity concentrations . . . . . 40
33	Lateral stress as a function of depth at 1.0 nanosecond for the keV, cal/cm <sup>2</sup> source incident upon the 300Å thick surface impurity layer with triple impurity concentrations . . . . . 41
34	Temperature as a function of depth at specific times for the 2 keV, 1 cal/cm <sup>2</sup> source incident upon the beryllium substrate (no surface impurity layer) . . . . . 42

<u>Figure</u>	<u>Page</u>
35	Temperature as a function of depth at specific times for the 2 keV, 1 cal/cm <sup>2</sup> source incident upon the 300Å thick surface impurity layer with the base impurity concentrations . . . . . 43
36	Temperature as a function of depth at specific times for the 2 keV, 1 cal/cm <sup>2</sup> source incident upon the 300Å thick surface impurity layer with triple impurity concentrations . . . . . 44
37	Energy deposited as a function of depth for the 2 keV, 5 cal/cm <sup>2</sup> source incident upon the beryllium substrate (no surface impurity layer) . . . . . 45
38	Energy deposited as a function of depth for the 2 keV, 5 cal/cm <sup>2</sup> source incident upon the 300Å thick surface impurity layer with the base impurity concentrations . . . . . 46
39	Energy deposited as a function of depth for the 2 keV, 5 cal/cm <sup>2</sup> source incident upon the 300Å thick surface impurity layer with triple impurity concentrations . . . . . 47
40	Axial stress as a function of depth at 1.0 nanosecond for the 2 keV, 5 cal/cm <sup>2</sup> source incident upon the beryllium substrate (no surface impurity layer) . . . . . 48
41	Lateral stress as a function of depth at 1.0 nanosecond for the 2 keV, 5 cal/cm <sup>2</sup> source incident upon the beryllium substrate (no surface impurity layer) . . . . . 49
42	Axial stress as a function of depth at 1.0 nanosecond for the 2 keV, 5 cal/cm <sup>2</sup> source incident upon the 300Å thick surface impurity layer with the base impurity concentrations . . . . . 50
43	Lateral stress as a function of depth at 1.0 nanosecond for the 2 keV, 5 cal/cm <sup>2</sup> source incident upon the 300Å thick surface impurity layer with the base impurity concentrations . . . . . 51
44	Axial stress as a function of depth at 1.0 nanosecond for the 2 keV, 5 cal/cm <sup>2</sup> source incident upon the 300Å thick surface impurity layer with triple impurity concentrations . . . . . 52
45	Lateral stress as a function of depth at 1.0 nanosecond for the 2 keV, 5 cal/cm <sup>2</sup> source incident upon the 300Å thick surface impurity layer with triple impurity concentrations . . . . . 53

<u>Figure</u>	<u>Page</u>
46	Temperature as a function of depth at specific times for the 2 keV, 5 cal/cm <sup>2</sup> source incident upon the beryllium substrate (no surface impurity layer) . . . . . 54
47	Temperature as a function of depth at specific times for the 2 keV, 5 cal/cm <sup>2</sup> source incident upon the 300Å thick surface impurity layer with the base impurity concentrations . . . . . 55
48	Temperature as a function of depth at specific times for the 2 keV, 5 cal/cm <sup>2</sup> source incident upon the 300Å thick surface impurity layer with triple impurity concentrations . . . . . 56



## ABSTRACT

Calculations were performed using the PUFF-TFT code to determine the thermo-mechanical response arising from incident mono-energetic X-rays on a beryllium substrate with a thin (300Å) impurity layer. The impurities were introduced into the material during typical fabrication processes. Responses were calculated for 5 nanosecond square wave pulses of monoenergetic X-rays (1 and 2 keV) with fluence levels corresponding to surface loadings of 1 and 5 cal/cm<sup>2</sup>. The presence of these surface impurities was found to significantly alter the thermal response of the medium. As the concentration of surface impurities increased, the energy deposition increased, and the temperature gradient increased. In some cases, additional impurities resulted in a phase change in the medium. For the most part, the mechanical response was unaffected by the surface impurity concentration.



# 1. INTRODUCTION

When a surface is polished to attain a high degree of reflectivity, small amounts of impurities are introduced into the material substrate. These impurities may have an insignificant effect on the optical properties of the medium, and their presence may be considered negligible. However, in the presence of incident X-rays, the impurity concentrations may be large enough to generate an energy deposition gradient of sufficient magnitude to induce stresses that result in deformation of the geometry or result in a phase change in the material, thereby altering the reflective properties of the medium.

The presence of the surface impurities affects not only the survivability of the mirror, but also impacts the machining process. For example, if the surface impurity concentrations play a minimal role in the hydrodynamic or thermal response of the medium, then other, less expensive or faster machining processes may be utilized. Conversely, stricter process control may be in order if the existence of surface impurities is considered detrimental.

This report examines the effect of a thin layer of surface impurities on the hydrodynamic response of a mirrored beryllium surface. To gauge the severity of the response, identical calculations were performed for beryllium media without surface impurities (bulk impurities only) and with triple impurity concentrations in the surface layer. Impurity concentrations, for both the surface layer and bulk impurities, were obtained by Rutherford backscatter spectrometry.

Results for this study were generated using a hydrodynamic computer code, or hydrocode. Hydrocodes solve the set of differential equations arising from the conservation of mass, momentum, and energy, coupled with an equation of state and a constitutive relation. The equation of state relates the materials density (or volume) and internal energy (or temperature) with pressure. A constitutive relation describes the particular nature of the material by relating the stress in the material with the amount of distortion (strain) required to produce this stress. The constitutive relation may include strain rate effects, work hardening, thermal heating/softening, etc.

The formulation of the differential equations follow either Eulerian or Lagrangian descriptions. The Eulerian description is a spatial description; the Lagrangian is a material description. In an Eulerian framework, all grid points, and consequently cell boundaries, remain fixed with time. Mass, momentum, and energy flow across cell boundaries. In a Lagrangian description, the grid points are attached to the material and move with the material. In this formulation, mass within a cell is invariant, but the volume of the cell may change with time because of expansion or compression of the material.

In the theory of elasticity, a material will undergo complete recovery from the strained state to the undeformed configuration upon removal of the applied loads. A one-to-one stress-strain relationship exists; the stress-strain-state point moves along the same characteristic curve for load increases or decreases. When stress intensities exceed a certain threshold value known as the elastic limit, or yield

stress, the deformation becomes permanent, and a transition is made to the plastic region. Now upon unloading a permanent plastic strain remains.

The remainder of this paper discusses the numerical methodology employed in this study to characterize the thermo-mechanical response of the medium, including a discussion of the input parameters and their values (Section 2), the presentation of the results and discussion (Section 3), and conclusions (Section 4).

## 2. METHODOLOGY

The PUFF-TFT code was used to assess the hydrodynamic response of a beryllium substrate with a thin surface impurity layer. The coupling of the TFT (Thin Film Transport) module with the PUFF74 code has been performed by Ktech Corporation.<sup>1</sup> The TFT package accounts for the effects of dose enhancement due to the transport of secondary particles with ranges comparable to the thickness of the thin material layers and thermal conduction between thin material layers. These two modifications (among others) more accurately portray the degree of energy sharing between thin layers, thereby modifying the expected energy depositions based on normal X-ray interactions and possibly altering the anticipated thermo-mechanical response of the medium.

The PUFF74 code,<sup>2</sup> originally developed in the mid-sixties, has undergone a number of revisions to become a flexible material response code that includes the effects of material strength, porosity, and fracture for both homogeneous and composite materials. The code calculates stress wave formation and propagation by numerical integration of the conservation equations in a one-dimensional Lagrangian coordinate system. In addition to the hydrodynamic equation of state, which is required for all materials, the code contains an elastic-plastic model for strength effects, a  $P$ - $\alpha$  porosity model for treating irreversible compaction, and four models for treating strain-rate dependent or dispersive effects.

This study examines the effect of a thin (300Å) surface impurity layer on the response of a beryllium substrate to incident monoenergetic X-rays. The substrate was arbitrarily subdivided into two layers of thickness 0.0001 cm and 0.01 cm for calculational purposes. Elemental concentrations of the surface impurity layer and beryllium substrate are provided in Table 1. Thermo-mechanical responses were calculated for 5 nanosecond square wave pulses of monoenergetic X-rays (1 and 2 keV) with fluence levels corresponding to surface loadings of 1 and 5 cal/cm<sup>2</sup>. X-ray temperatures and fluence levels were varied to better characterize the material response.

Of great importance to a material response code are the values of the input parameters. Aside from the usual parameters such as density, latent heats of vaporization and fusion, etc., the PUFF-TFT code requires coefficients for quadratic equations modeling thermal conductivity and specific heat, coefficients for the cubic equation modeling the Hugoniot data, yield strength, shear modulus, and a host of additional input values. Input values are also required for porosity models and dispersive medium models, if these options are selected. The significance of this is the difficulty in obtaining accurate values for these parameters. In many cases, such data is unavailable and values must be assumed. As is well known, code results are only as good as the code input.

Material property data for this analysis was generally taken from three sources. Most of the thermophysical data was taken from Childs.<sup>3,4</sup> The equation of state (EOS) data was obtained from Rice.<sup>5</sup> Values for the remaining material property input parameters were obtained from Sauer.<sup>6</sup> A complete PUFF-TFT input deck

Table 1.  
Material Compositions  
(mass fraction)

Element	Bulk	300Å Surface Layer	
		1X	3X
Be	0.9928	0.8460	0.5374
C		0.0243	0.0729
O	0.0035	0.1013	0.3039
F		0.0096	0.0288
Al	0.0030	0.0034	0.0102
Si		0.0036	0.0108
P		0.0023	0.0069
S		0.0024	0.0072
Cl		0.0018	0.0054
Cr		0.0039	0.0117
Fe	0.0006		
Cu		0.0016	0.0048

is provided as Appendix A. Note that the equation of state data is unchanged for both material types, i.e., the thin impurity layer and the beryllium substrate. The presence of the increased impurity concentrations was not considered significant enough to warrant an extensive literature search for revised EOS or thermophysical input data.

### 3. RESULTS AND DISCUSSION

Three geometries were considered in this study: case 1, a beryllium slab with bulk impurities; case 2, a beryllium slab with bulk impurities and a 300Å thick impurity layer; and case 3, a beryllium slab with bulk impurities and a 300Å thick layer with impurity concentrations 3 times those of case 2. There were four permutations on X-ray sensitivity for each geometry: two temperatures, 1 and 2 keV, and two fluences, 1 and 5 cal/cm<sup>2</sup>, were considered. The problem was initiated at time 0.0 with a 5.0 nanosecond square-wave X-ray pulse.\* In each PUFF-TFT run, detailed edits and plots were requested at 7 times: 0.1, 0.5, 1.0, 2.0, 3.0, 4.0, and 5.0 nanoseconds after problem initiation. At each edit, tabular data was listed for 20 variables. The mesh spacing for cases 2 and 3 was extremely small, with cell sizes ranging from 20 Å near the front surface to 5 μm at the back surface. Approximately 160 mesh cells were required for these geometries.

To minimize the amount of data presented in this report, it was decided to focus on graphical output, resorting to tabular data only when necessary. Plots have been prepared for energy deposition as a function of depth; for axial and lateral stresses, temperature, and dose/enthalpy as a function of depth at each of the above listed times; and for axial and lateral stresses and temperature versus time at specific locations in the medium. Not all of the data available will be presented in this report. Only those plots that illustrate the thermo-mechanical response of the medium will be utilized.

#### 3.1 SOURCE TERM NO. 1: 1 keV, 1 cal/cm<sup>2</sup>

This will be the reference source term: a temperature of 1 keV and a surface loading of 1 cal/cm<sup>2</sup>. Figures 1 through 3 depict the energy deposition for the three geometries: case 1, case 2, and case 3, respectively. The significance of the impurities in the surface layer is clearly evident. The dose received by the geometry with the triple concentration of surface impurities is nearly four times that of the dose to the bulk material. The dose enhancement effect is also shown, illustrating the energy transported out of the surface layer into the bulk material by secondary particles. The dotted line in these figures represents the dose received by the material if particle transport were neglected.

With such a significant difference in energy deposition, some change in the material response may be anticipated. Two competing effects are examined. At early times, the stress response is predominant in the surface layer. The axial stress wave moves into the material at approximately the speed of sound, quickly passing through the thin surface layer. For each geometry, the lateral stresses have reached and exceeded the yield stress, 4 kbar, for the material, indicating the generation of permanent plastic strains. The transition to the plastic regime may indicate some deterioration in the optical properties of the medium. Figures 4 through 9 show the

---

\* The use of a square wave pulse resulted in conservative estimates of the peak stresses and peak temperatures.

axial and lateral stress waves for each geometry at 0.5 nanoseconds. The vertical dashed lines in each of these figures denote material interfaces. Recall that the beryllium substrate has been subdivided into two layers of 0.01 and 0.0001 cm.

At longer times, temperature effects dominate the system. The temperature gradient follows the energy deposition gradient. Maximum temperatures are not obtained until the end of the energy deposition cycle at 5 nanoseconds. Figures 10 through 12 show the temperature for each geometry as a function of depth at specific times. The increase in temperature as a function of time is clearly shown for each geometry. What is most significant is the change in the temperature gradient and maximum temperature due to the increase in surface impurities. In the worst case, triple impurity concentrations, the surface temperature approaches the melting point.

To summarize the response of these geometries, it is noted: (a) the surface impurities do not play a significant role in the mechanical response of the media, i.e., magnitude and propagation of stresses; however, the yield point has been exceeded in all three cases; (b) the surface impurities contribute strongly to the thermal response, with temperatures approaching melting in the geometry with the highest surface impurity concentrations.

### **3.2 SOURCE TERM NO. 2: 1 keV, 5 cal/cm<sup>2</sup>**

This is the most stressing source term. The high fluence coupled with the low temperature means most of the energy is deposited in a very narrow range near the surface. Because of the magnitude of the energy deposition, the problem becomes less meaningful: even the bulk material shows considerable degradation, with melting occurring as early as 2 nanoseconds and axial and lateral stresses well in excess of yield point. The presence of the surface impurities magnifies these effects. At 2 nanoseconds there is extensive spallation for both the reference impurity concentration and triple impurity concentration, in addition to extensive melting. This is in contrast to the previous discussion where the impurity concentration was not a factor in the mechanical response. Figures 13 through 15 show the energy deposition for each case, Figures 16 through 21 show the axial and lateral stresses in the medium at 1 nanosecond, and Figures 22 through 24 show the temperature as a function of depth at specific times for each geometry.

### **3.3 SOURCE TERM NO. 3: 2 keV, 1 cal/cm<sup>2</sup>**

This is the most benign source term. The higher energy X-rays, because of smaller interaction cross sections, penetrate further into the material, thereby reducing the energy deposition and temperature gradients seen with the 1 keV, 1 cal/cm<sup>2</sup> source term. About 23% of the incident energy is now lost due to leakage from the back face, as compared to approximately 3% for the reference source. The dose enhancement is more clearly evident, reducing the magnitude of the energy deposited in the surface impurity layer and increasing the dose to the substrate. Axial and lateral stresses exceed the yield point, but the magnitudes are smaller and the time frame is longer, i.e., the transition to the plastic region occurs at later

times. There are no phase transitions; the maximum temperature remains below 250 °C. The presence of the impurities in the surface layer affects only the thermal response, as before. Figures 25 through 27 show the energy deposition for each case, Figures 28 through 33 show the axial and lateral stresses in the medium at 3 nanoseconds, and Figures 34 through 36 show the temperature as a function of depth at specific times for each geometry.

#### **3.4 SOURCE TERM NO. 4: 2 keV, 5 cal/cm<sup>2</sup>**

The thermal response of the media to this source was less than that from the 1 keV, 1 cal/cm<sup>2</sup> source. The magnitude of the mechanical response, however, is similar to the 1 keV, 5 cal/cm<sup>2</sup> source. The presence of the surface impurities did not alter the mechanical response significantly, and the temperature gradients and energy deposition gradient were smaller. There were no phase changes, but large axial and lateral stresses were calculated. Figures 37 through 39 show the energy deposition for each case, Figures 40 through 45 show the axial and lateral stresses in the medium at 1 nanosecond, and Figures 46 through 48 show the temperature as a function of depth at specific times for each geometry.

## 4. CONCLUSIONS

The purpose of this study was to ascertain the effect of surface impurities on the thermo-mechanical response of a beryllium medium. Although some impurities were already present in the material, polishing processes, etc., contributed additional impurities within a thin surface layer. To characterize the effect, impurity concentrations were parameterized. Three cases were examined: no additional surface impurities, a reference surface impurity concentration, and triple surface impurity concentration. The presence of these surface impurities was found to significantly alter the thermal response of the medium. As the concentration of surface impurities increased, the energy deposition increased, and the temperature gradient increased. In some cases, the additional impurities resulted in a phase change in the medium. For the most part, the mechanical response was unaffected by the surface impurity concentration. However, with one source, there was a large degree of spallation in the two cases with surface impurities and much less spallation in the geometry without the surface impurity layer.

One critical characteristic was noted in the mechanical response of the medium: stress levels exceeded the elastic limit of 4 kbar for each of the source terms and geometries. The transition from the elastic to the plastic regime results in permanent deformations within the material and the potential degradation of the optical properties of the medium.

One of the chief assumptions made in this effort was the invariance of the material properties with impurity concentration. There was no available information on this subject. But the question remains as to the effect of changes in elemental concentrations on the material properties. If the material properties are significantly altered by small changes in composition, then the results of this study are less valid. An associated question relates to the availability of material properties in general. In order to model physical systems, accurate data must be utilized. The absence of such data severely hampers the effort to characterize the response of a material to some external perturbation such as incident X-rays.

Future work will not only include one-dimensional material response studies, but will also investigate multi-dimensional effects. Material deformations can be more easily quantified with a multi-dimensional hydrocode. Ktech Corporation is currently preparing a TFF module for incorporation into a 2D hydrocode and this package, when available, will be used to further characterize radiation effects in thin films.

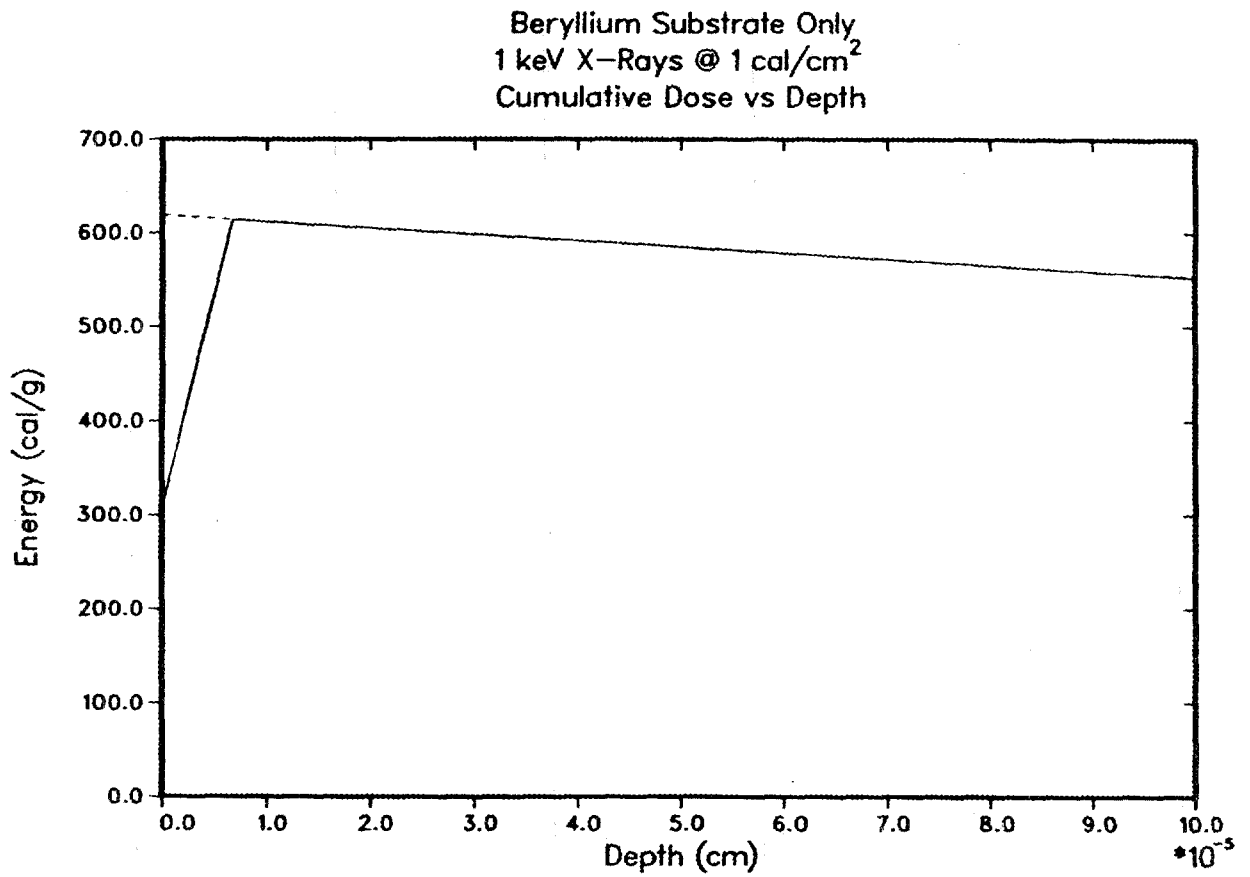


Figure 1. Energy deposited as a function of depth for the 1 keV, 1 cal/cm<sup>2</sup> source incident upon the beryllium substrate (no surface impurity layer).

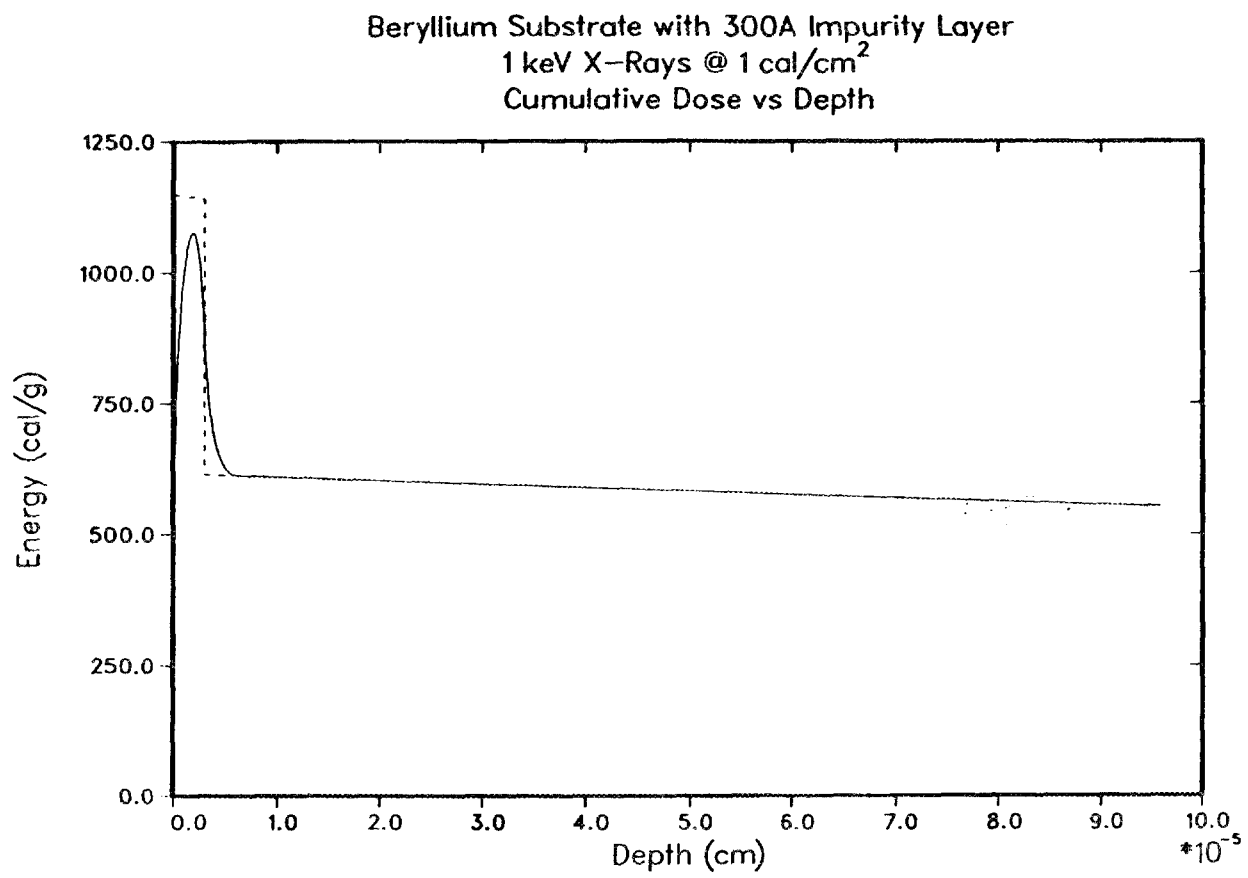


Figure 2. Energy deposited as a function of depth for the 1 keV, 1 cal/cm<sup>2</sup> source incident upon the 300Å thick surface impurity layer with the base impurity concentrations.

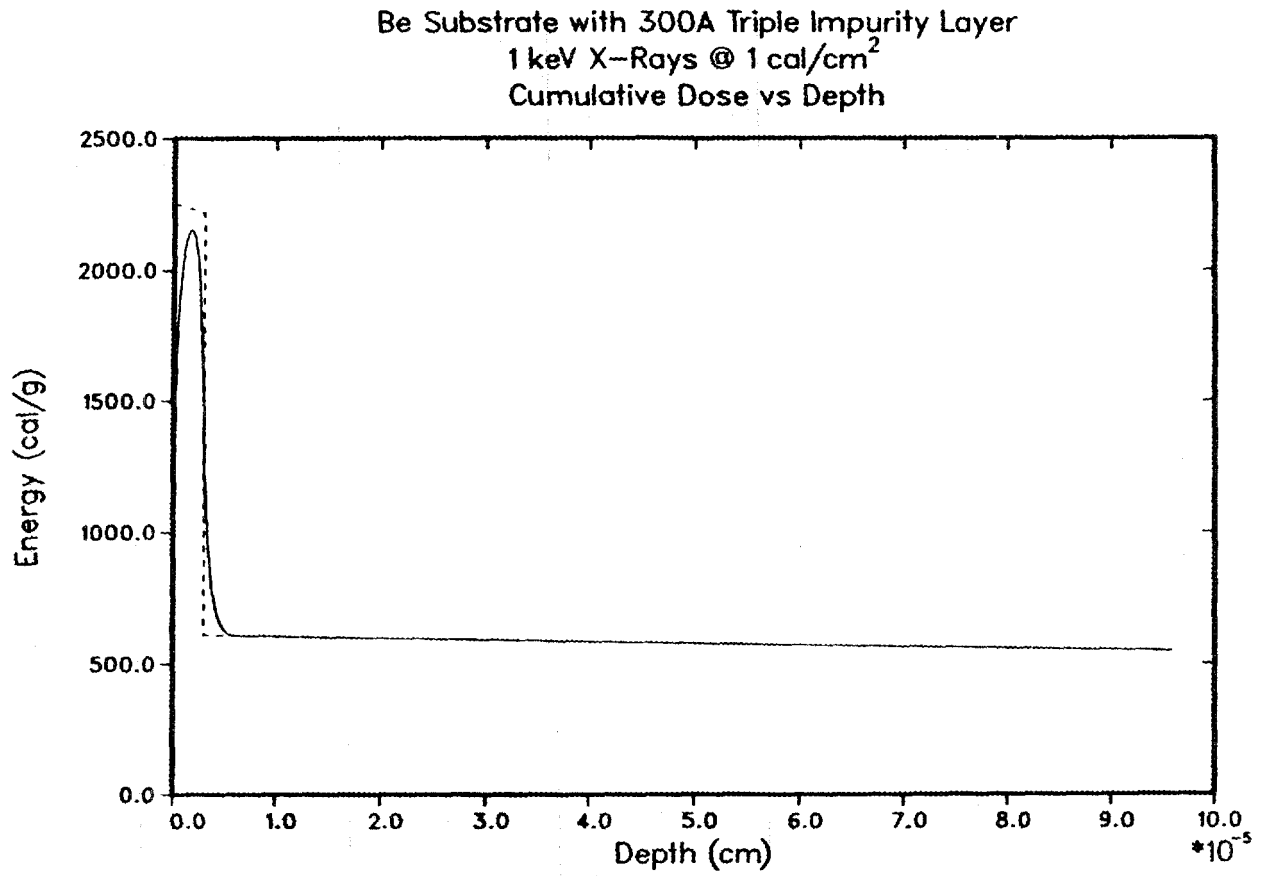


Figure 3. Energy deposited as a function of depth for the 1 keV, 1 cal/cm<sup>2</sup> source incident upon the 300Å thick surface impurity layer with triple impurity concentrations.

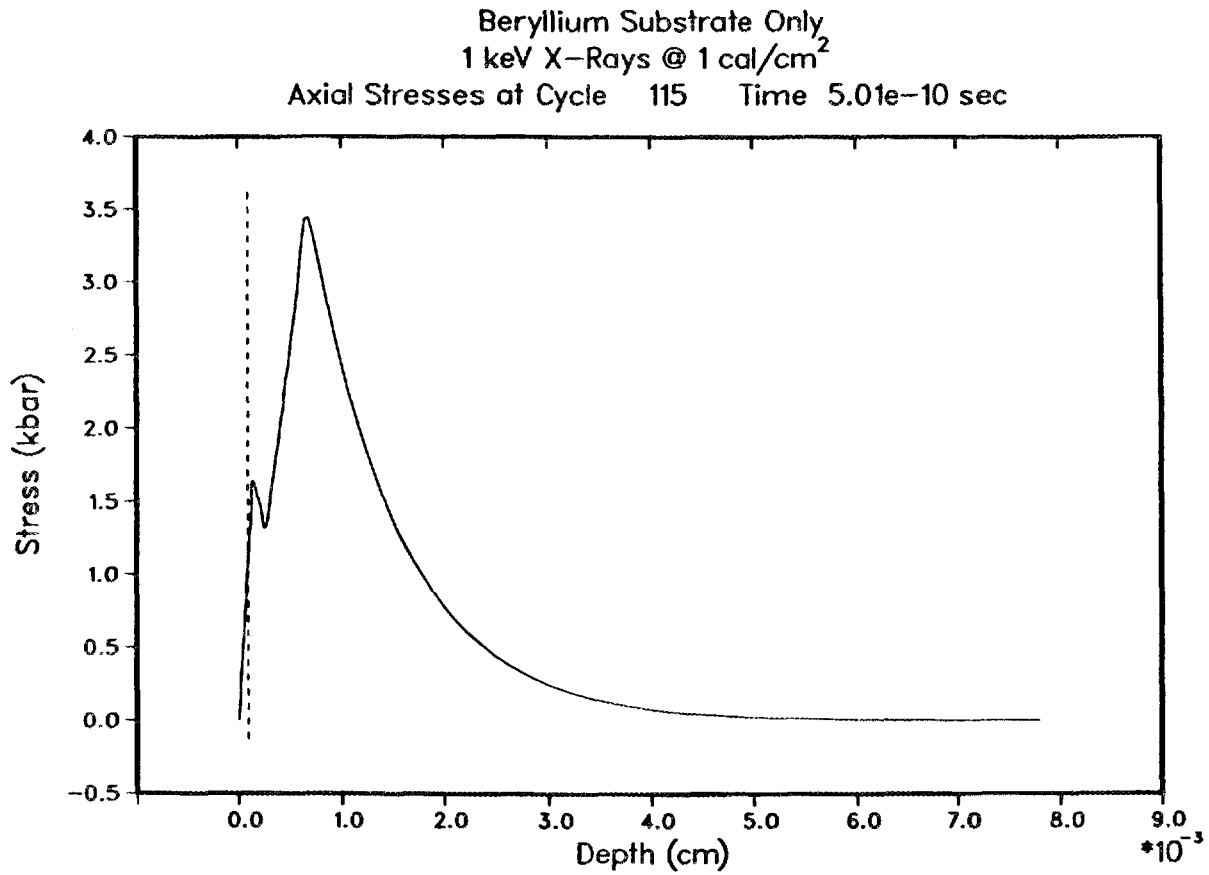


Figure 4. Axial stress as a function of depth at 0.5 nanosecond for the 1 keV, 1 cal/cm<sup>2</sup> source incident upon the beryllium substrate (no surface impurity layer).

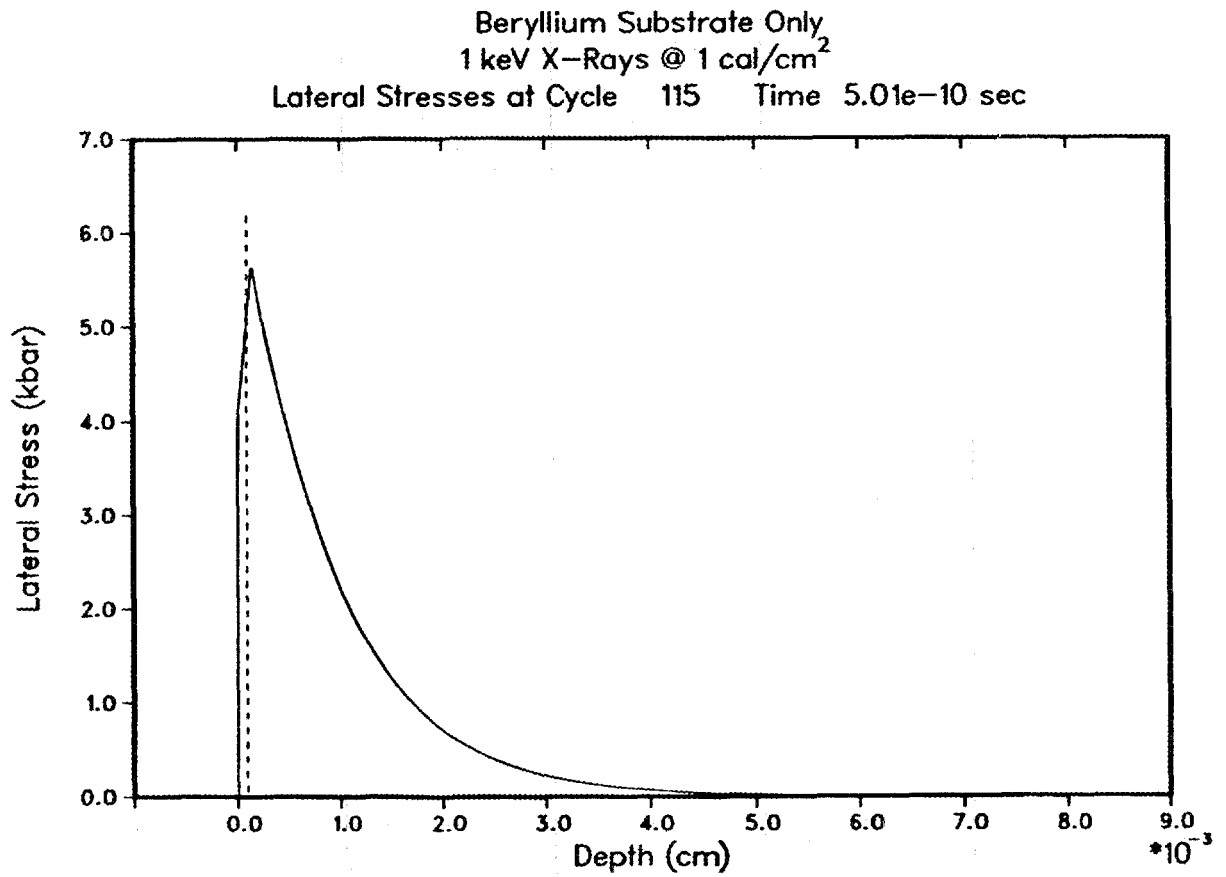


Figure 5. Lateral stress as a function of depth at 0.5 nanosecond for the 1 keV, 1 cal/cm<sup>2</sup> source incident upon the beryllium substrate (no surface impurity layer).

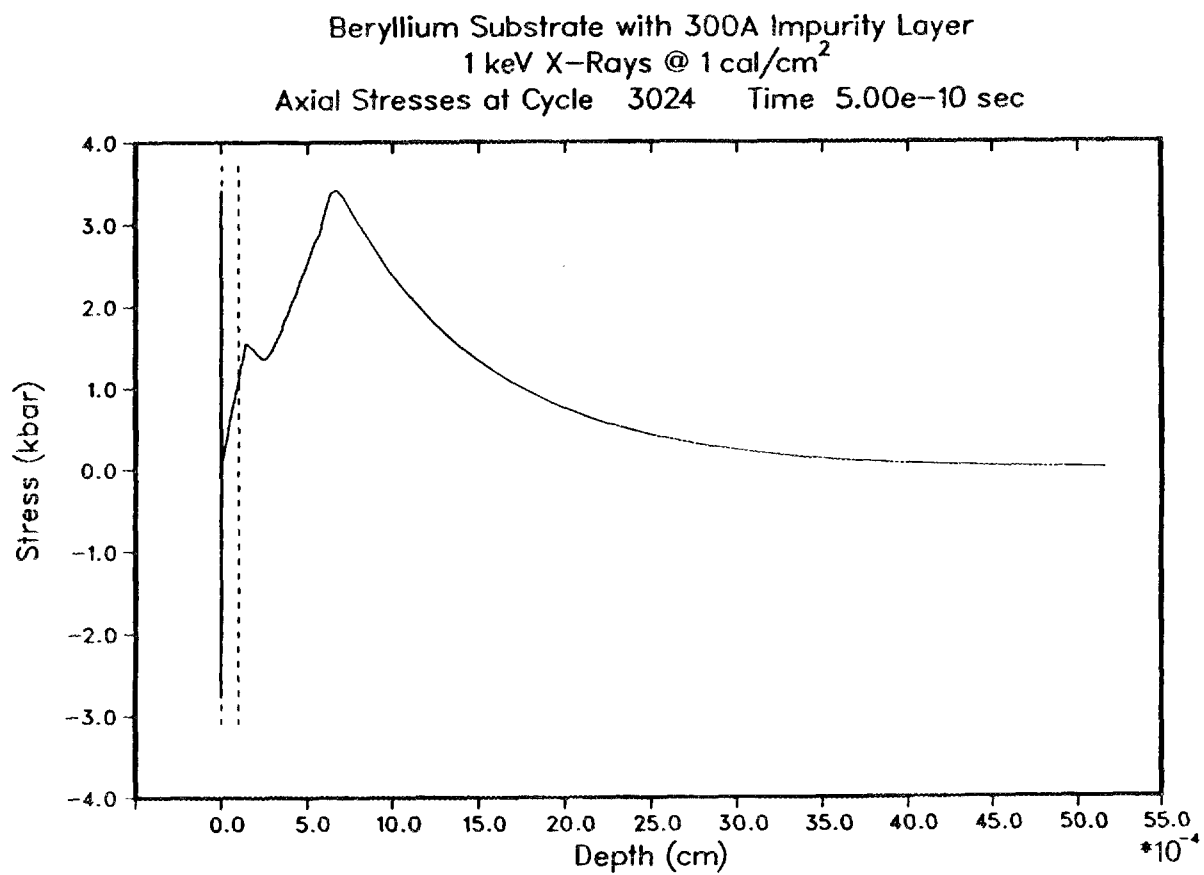


Figure 6. Axial stress as a function of depth at 0.5 nanosecond for the 1 keV, 1 cal/cm<sup>2</sup> source incident upon the 300Å thick surface impurity layer with the base impurity concentrations.

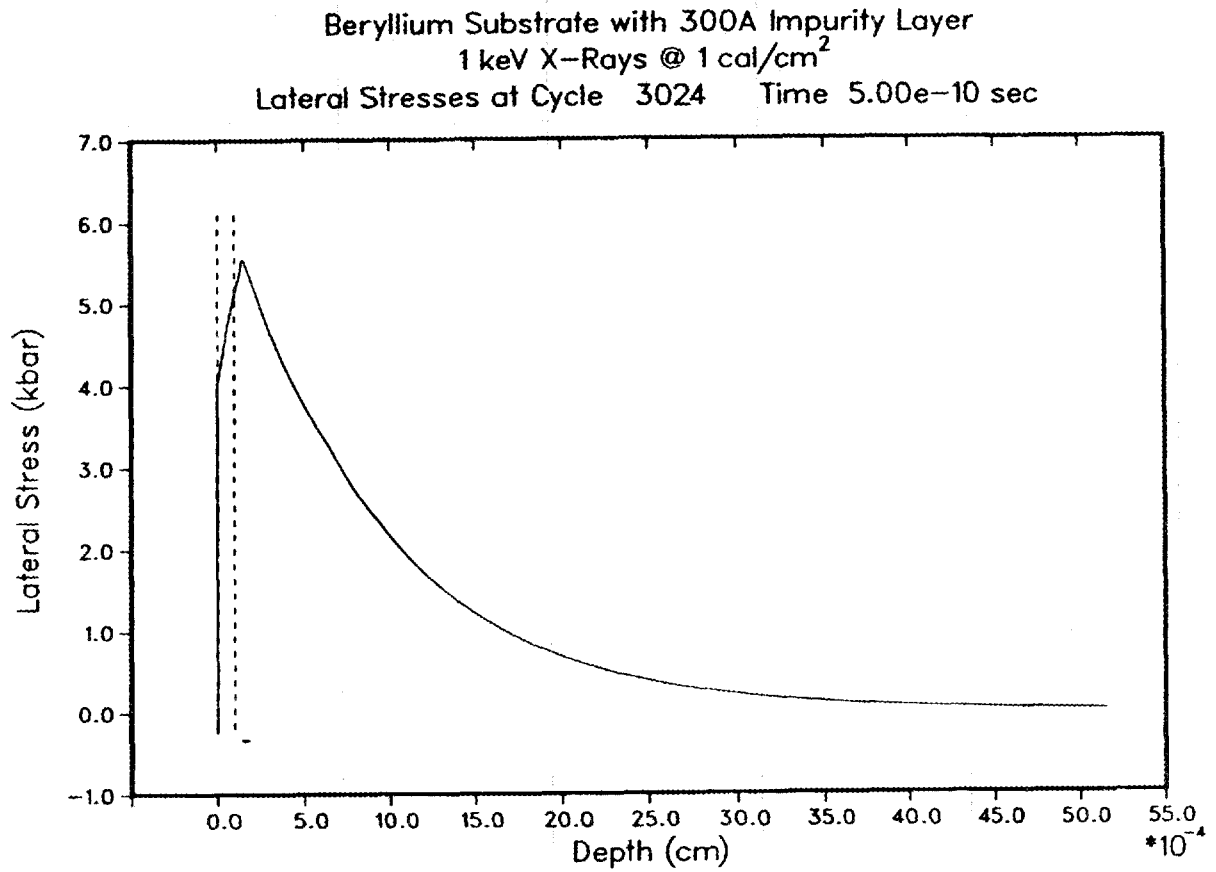


Figure 7. Lateral stress as a function of depth at 0.5 nanosecond for the 1 keV, 1 cal/cm<sup>2</sup> source incident upon the 300Å thick surface impurity layer with the base impurity concentrations.

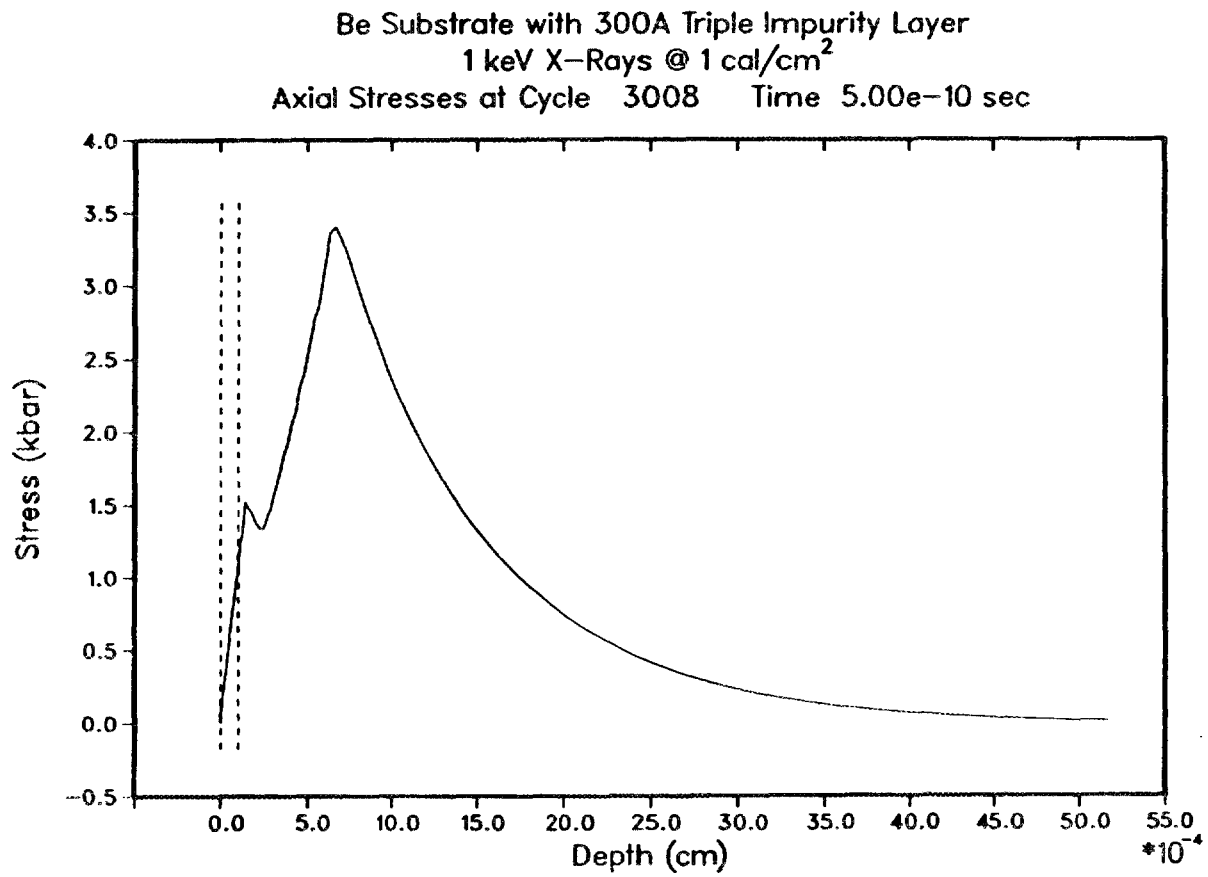


Figure 8. Axial stress as a function of depth at 0.5 nanosecond for the 1 keV, 1 cal/cm<sup>2</sup> source incident upon the 300Å thick surface impurity layer with triple impurity concentrations.

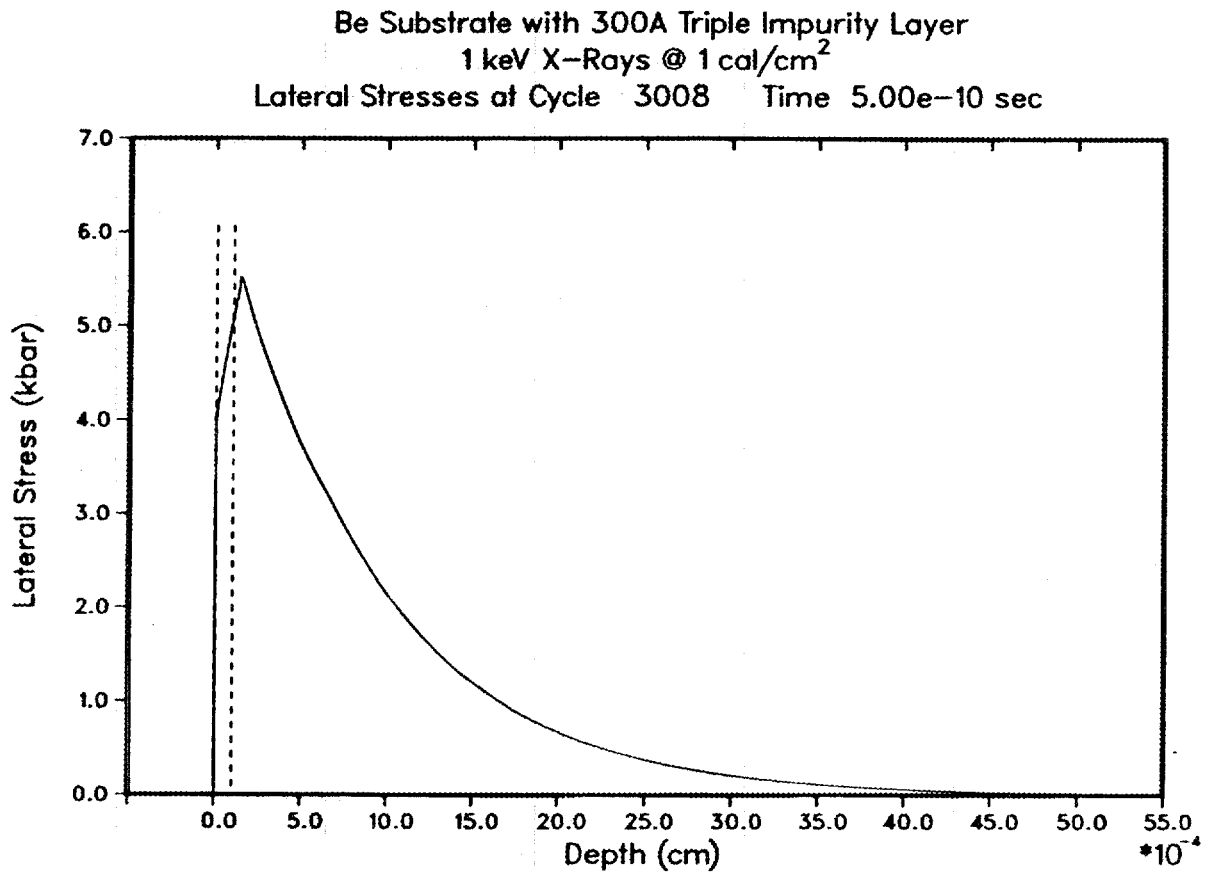


Figure 9. Lateral stress as a function of depth at 0.5 nanosecond for the 1 keV, 1 cal/cm<sup>2</sup> source incident upon the 300Å thick surface impurity layer with triple impurity concentrations.

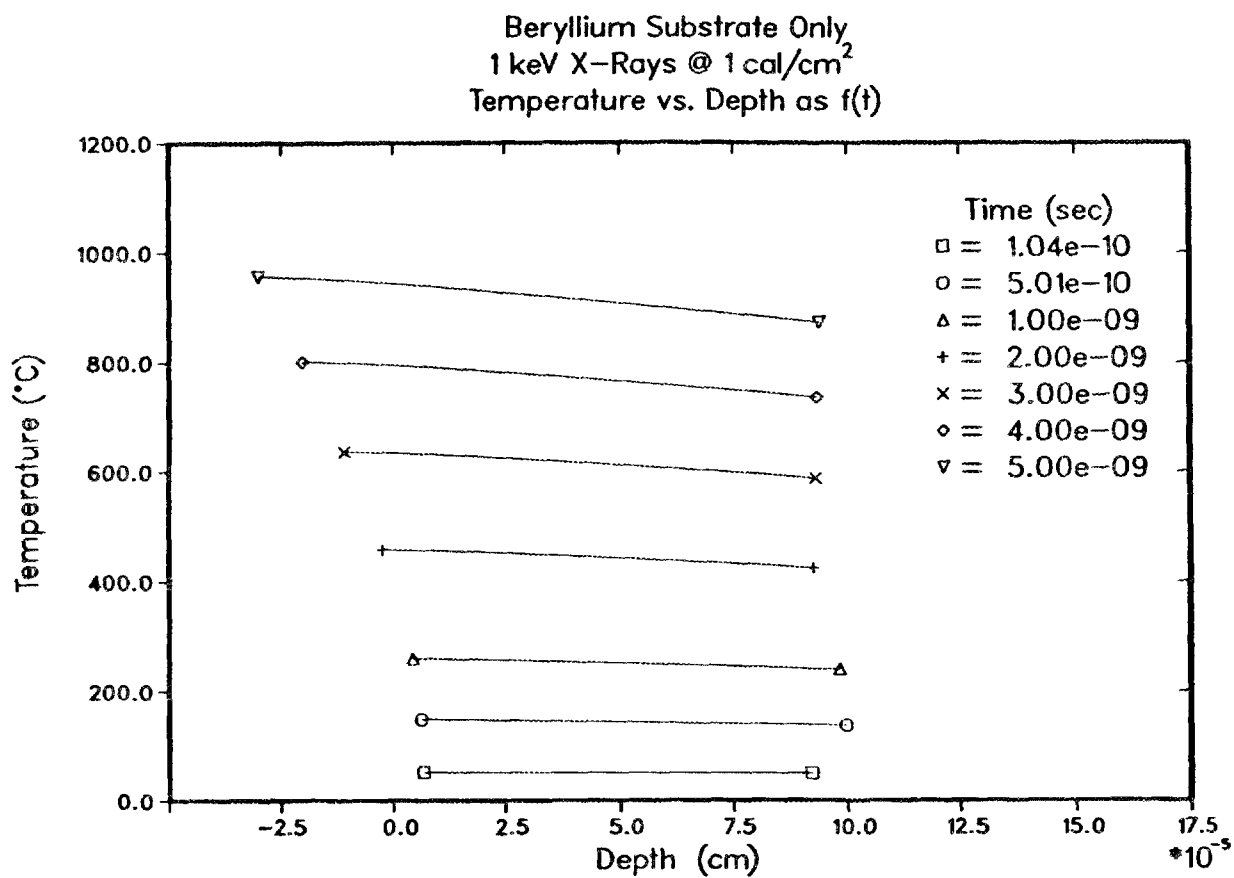


Figure 10. Temperature as a function of depth at specific times for the 1 keV, 5 cal/cm<sup>2</sup> source incident upon the beryllium substrate (no surface impurity layer).

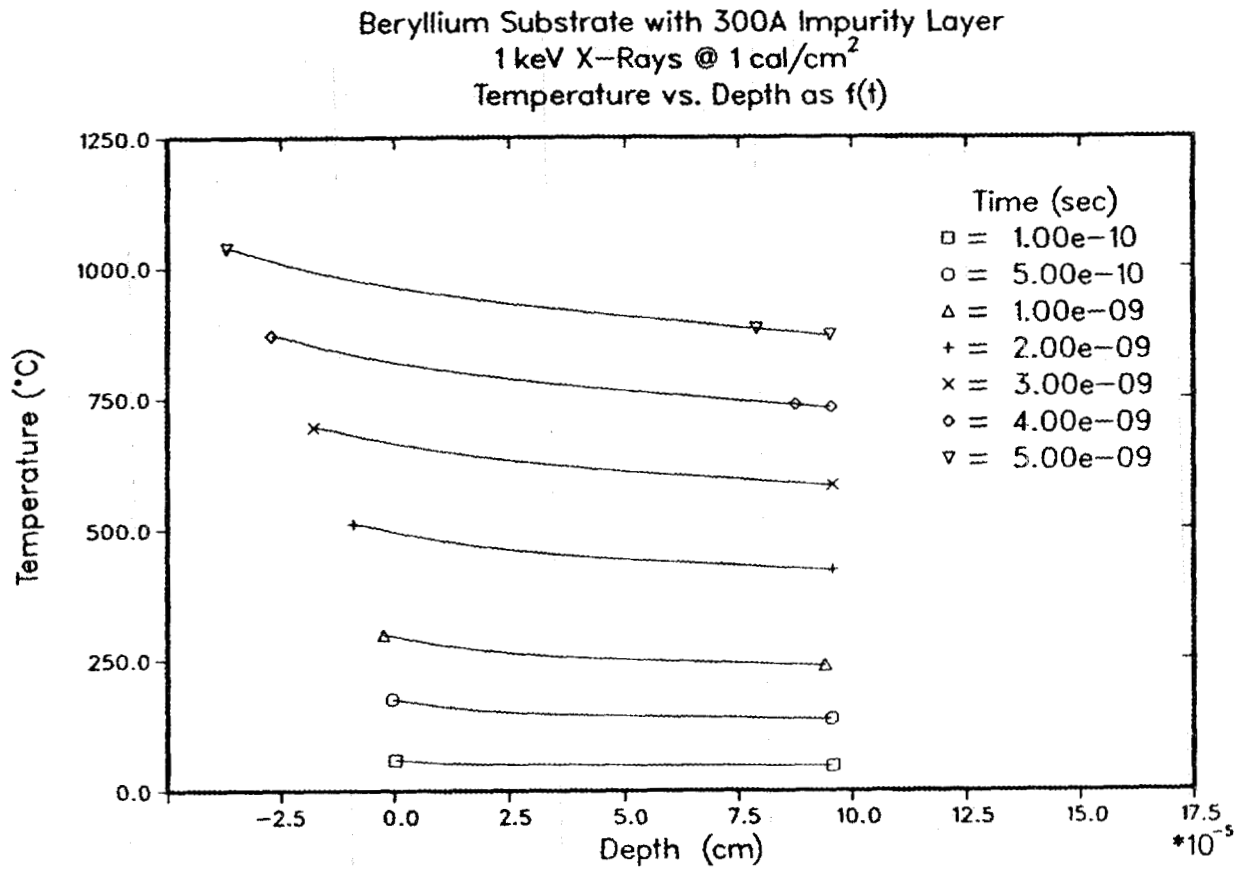


Figure 11. Temperature as a function of depth at specific times for the 1 keV, 5 cal/cm<sup>2</sup> source incident upon the 300Å thick surface impurity layer with the base impurity concentrations.

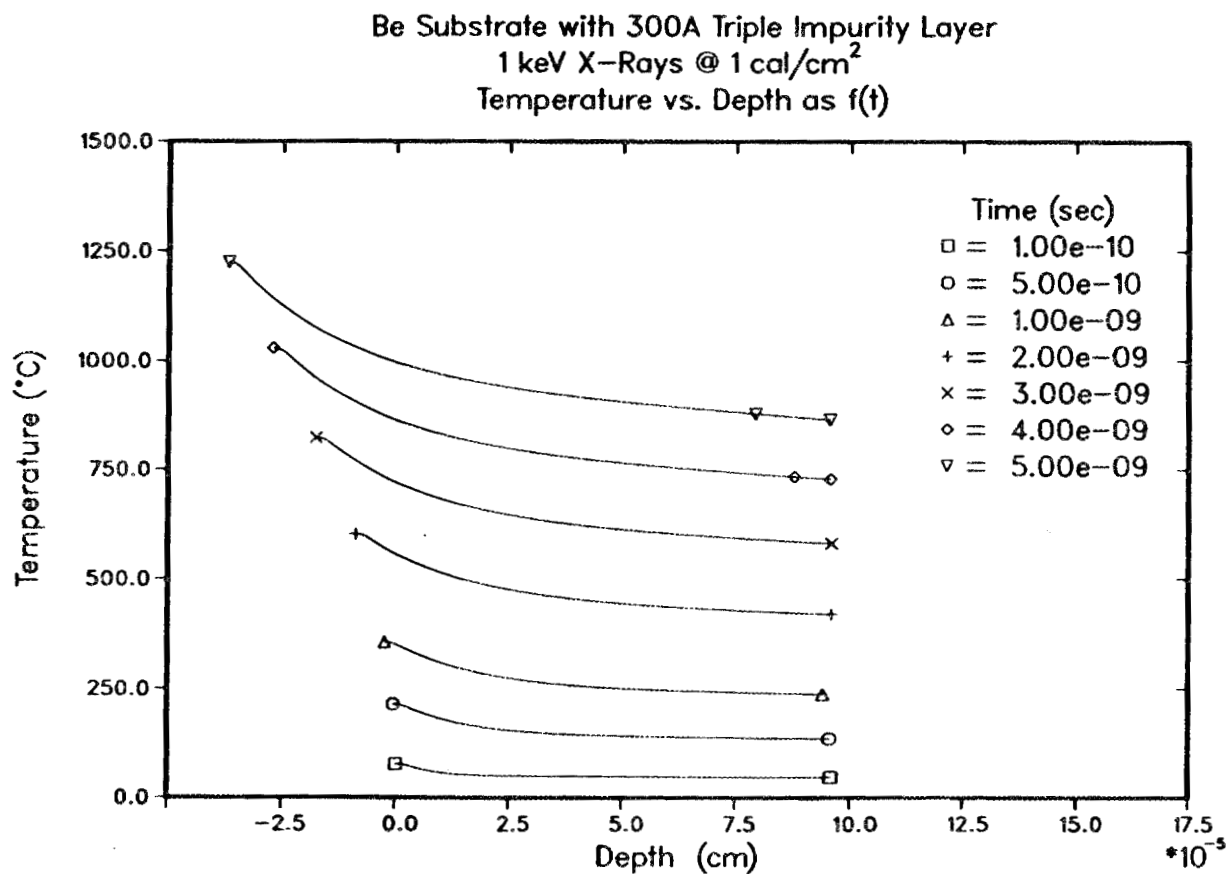


Figure 12. Temperature as a function of depth at specific times for the 1 keV, 5 cal/cm<sup>2</sup> source incident upon the 300Å thick surface impurity layer with triple impurity concentrations.

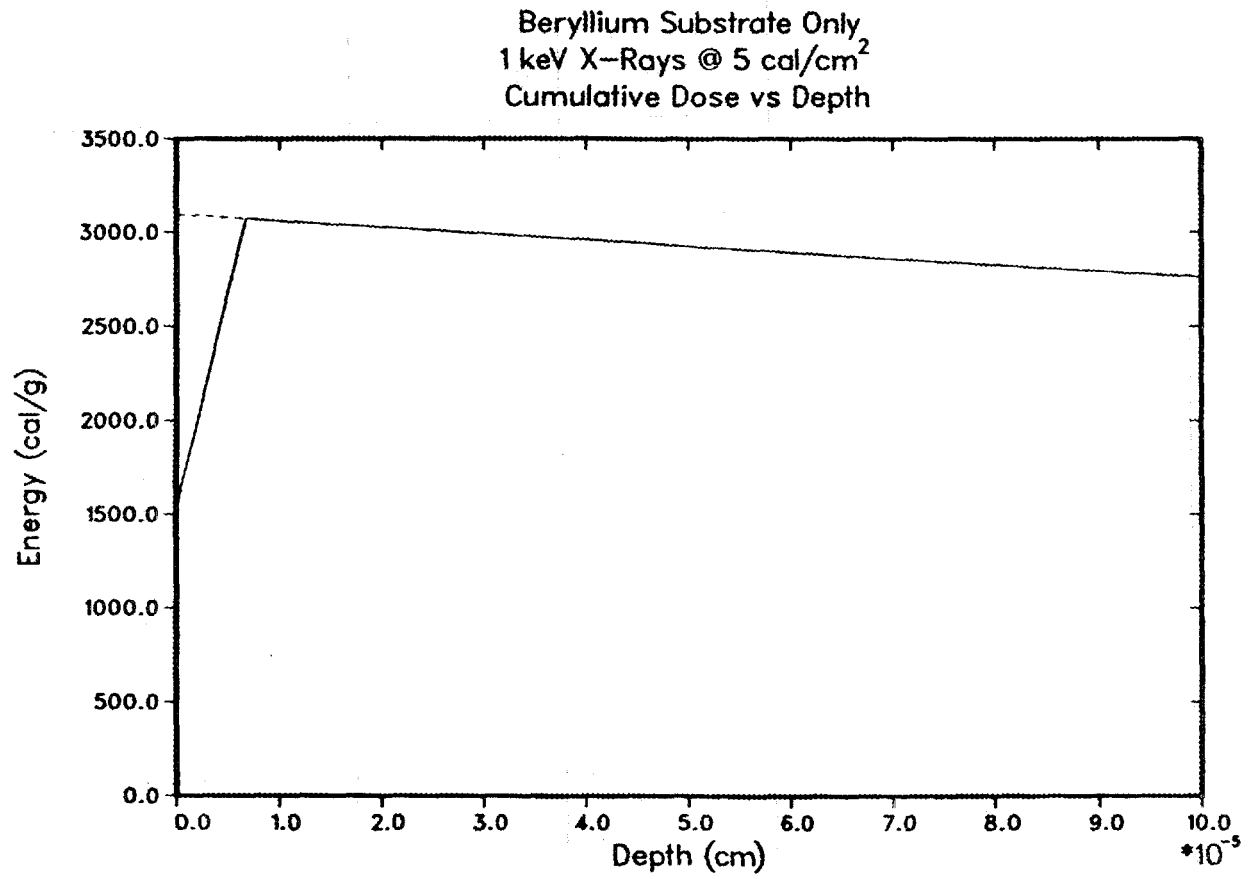


Figure 13. Energy deposited as a function of depth for the 1 keV, 5 cal/cm<sup>2</sup> source incident upon the beryllium substrate (no surface impurity layer).

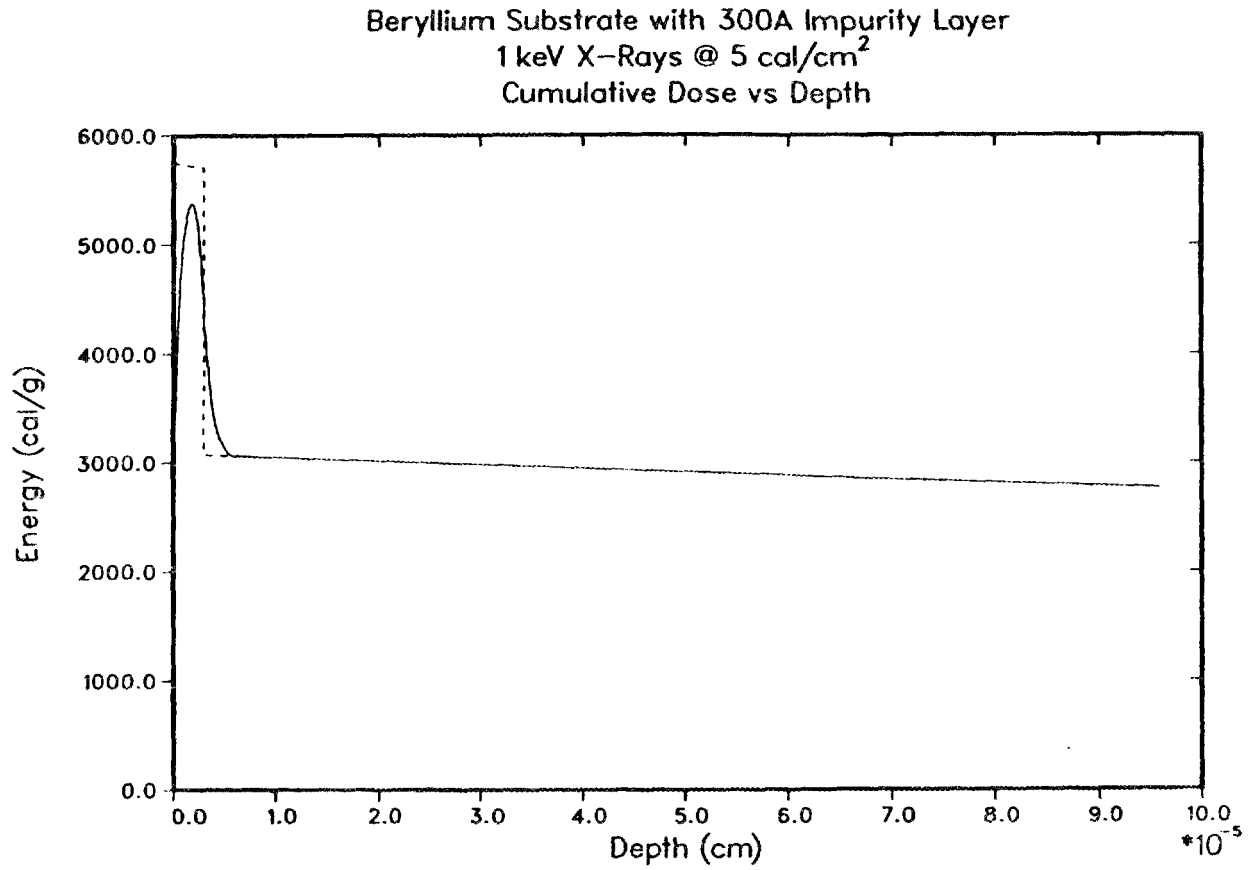


Figure 14. Energy deposited as a function of depth for the 1 keV, 5 cal/cm<sup>2</sup> source incident upon the 300Å thick surface impurity layer with the base impurity concentrations.

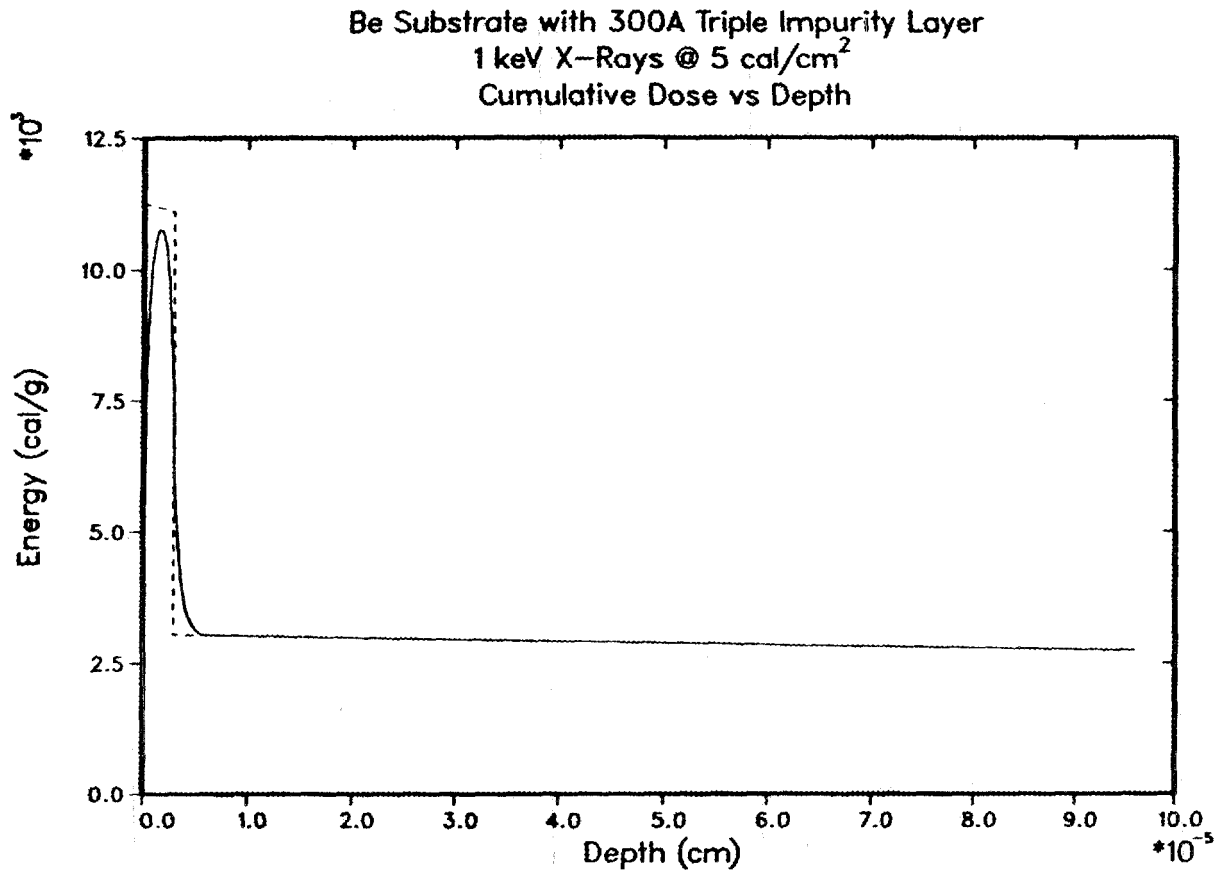


Figure 15. Energy deposited as a function of depth for the 1 keV, 5 cal/cm<sup>2</sup> source incident upon the 300Å thick surface impurity layer with triple impurity concentrations.

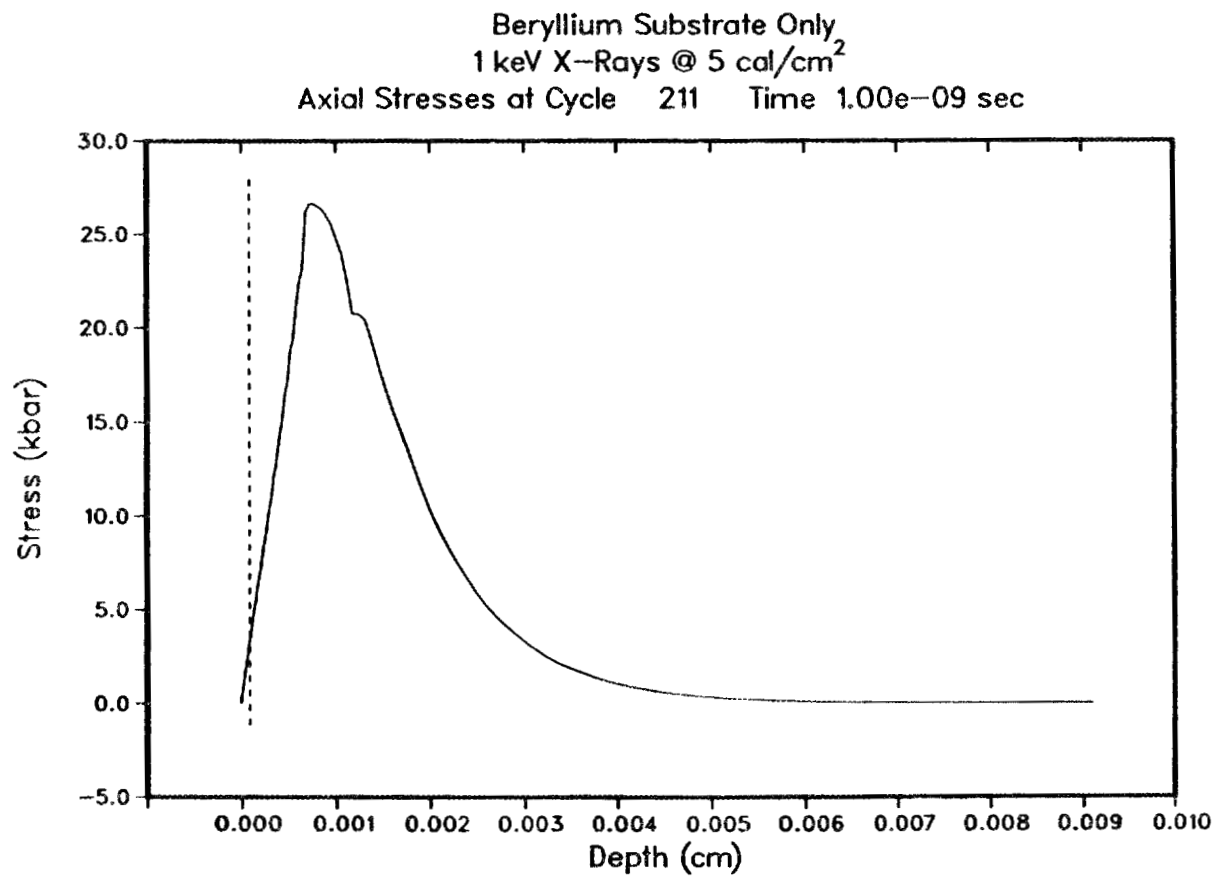


Figure 16. Axial stress as a function of depth at 1.0 nanosecond for the 1 keV, 5 cal/cm<sup>2</sup> source incident upon the beryllium substrate (no surface impurity layer).

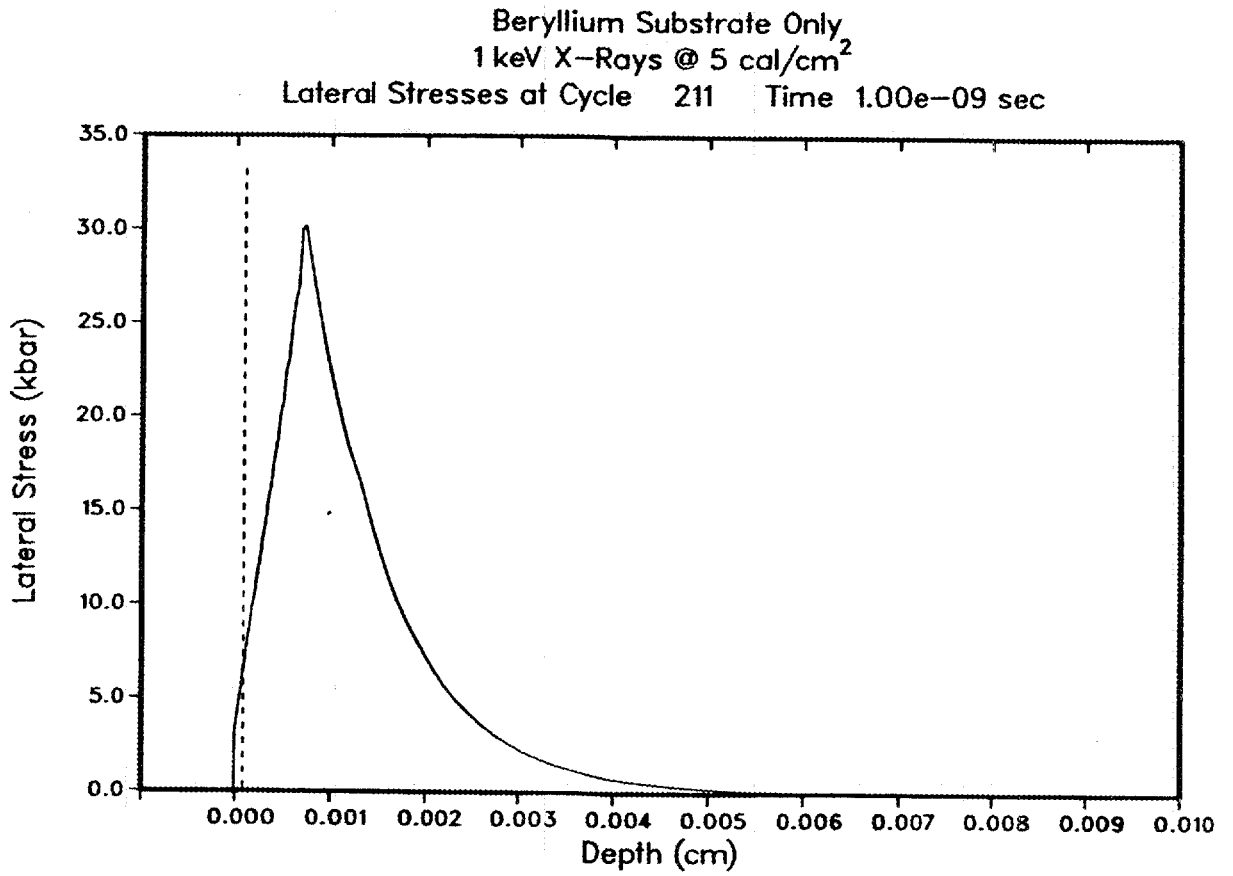


Figure 17. Lateral stress as a function of depth at 1.0 nanosecond for the 1 keV, 5 cal/cm<sup>2</sup> source incident upon the beryllium substrate (no surface impurity layer).

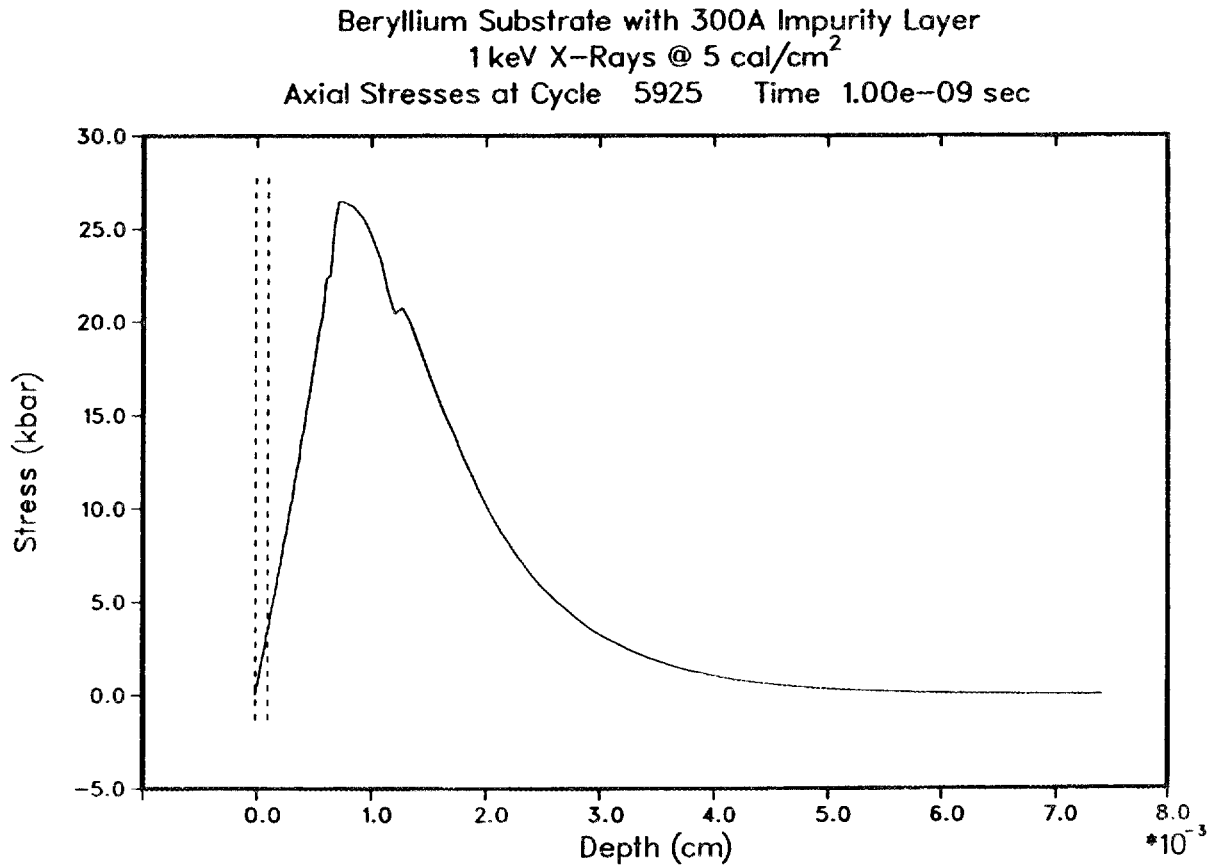


Figure 18. Axial stress as a function of depth at 1.0 nanosecond for the 1 keV, 5 cal/cm<sup>2</sup> source incident upon the 300Å thick surface impurity layer with the base impurity concentrations.

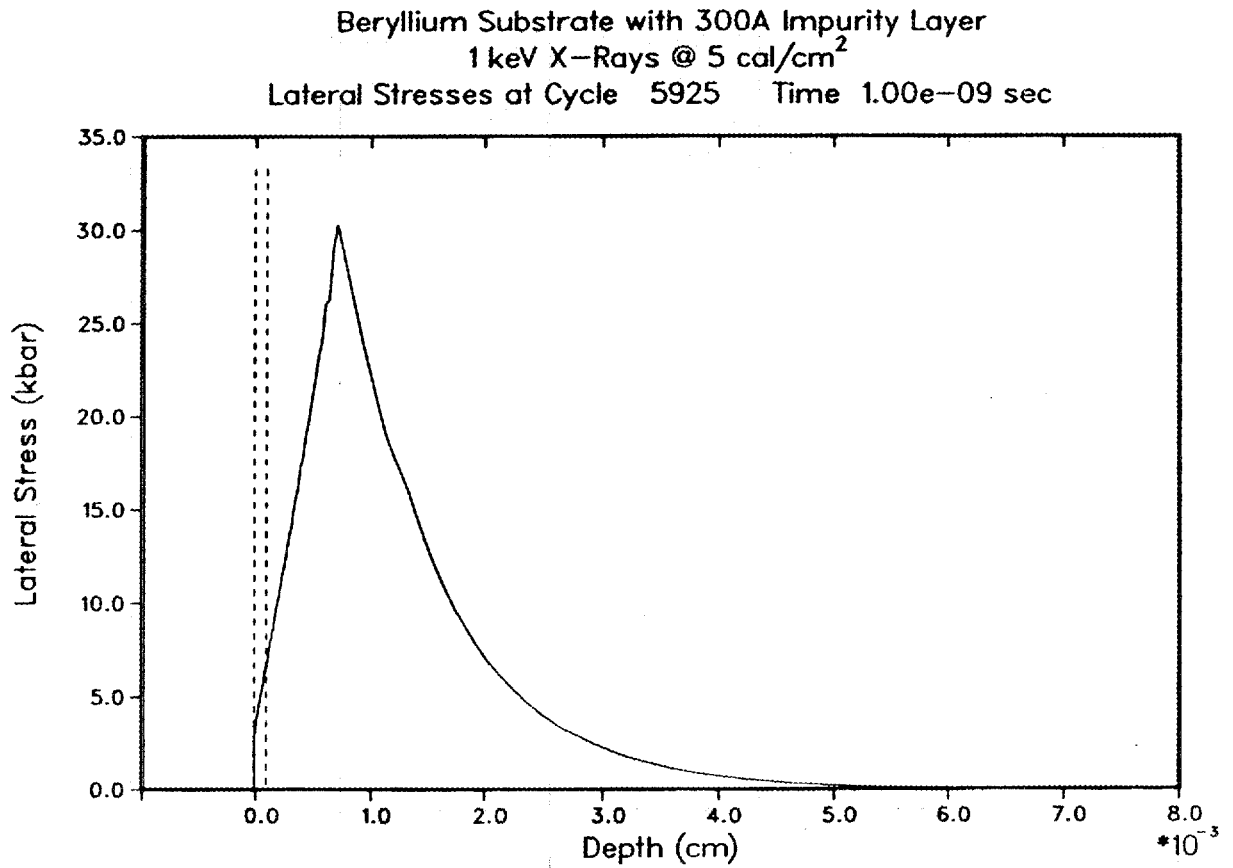


Figure 19. Lateral stress as a function of depth at 1.0 nanosecond for the 1 keV, 5 cal/cm<sup>2</sup> source incident upon the 300Å thick surface impurity layer with the base impurity concentrations.

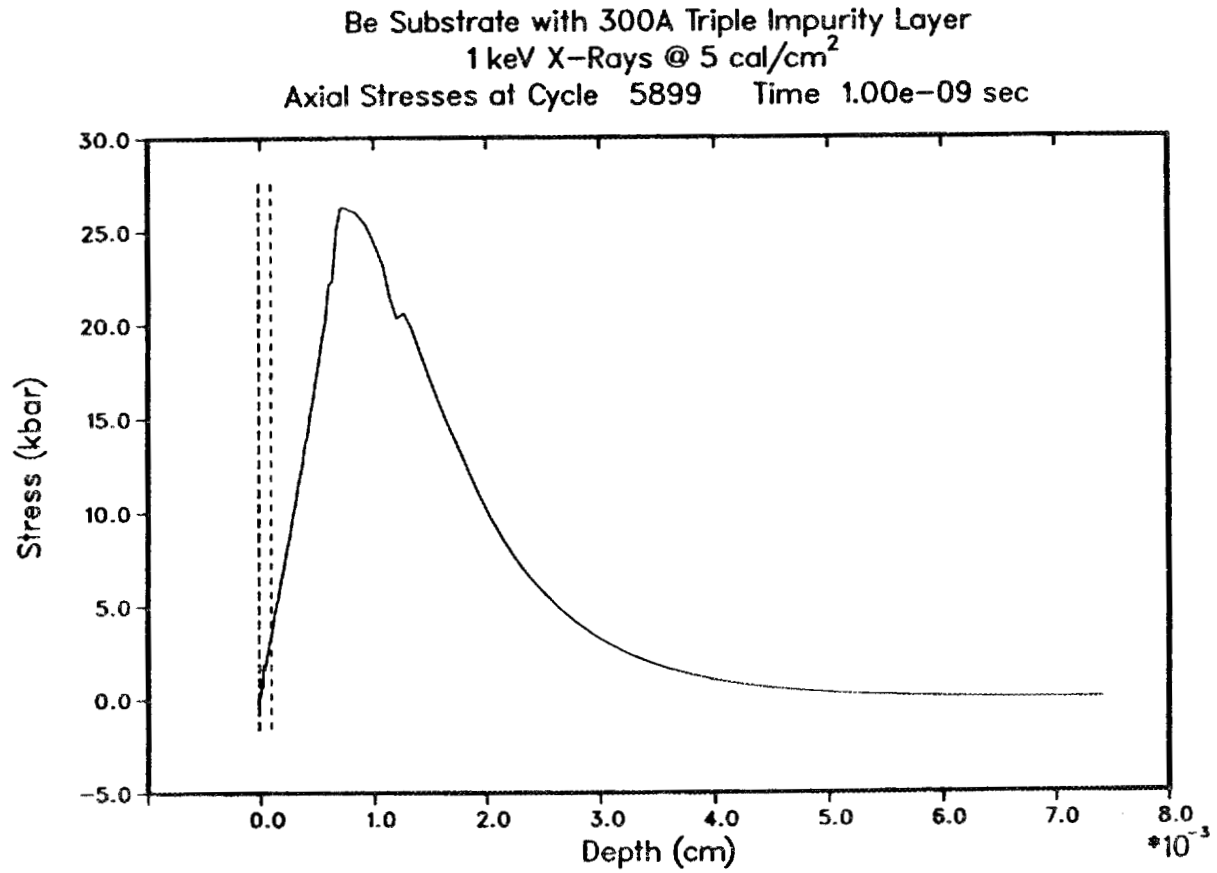


Figure 20. Axial stress as a function of depth at 1.0 nanosecond for the 1 keV, 5 cal/cm<sup>2</sup> source incident upon the 300Å thick surface impurity layer with triple impurity concentrations.

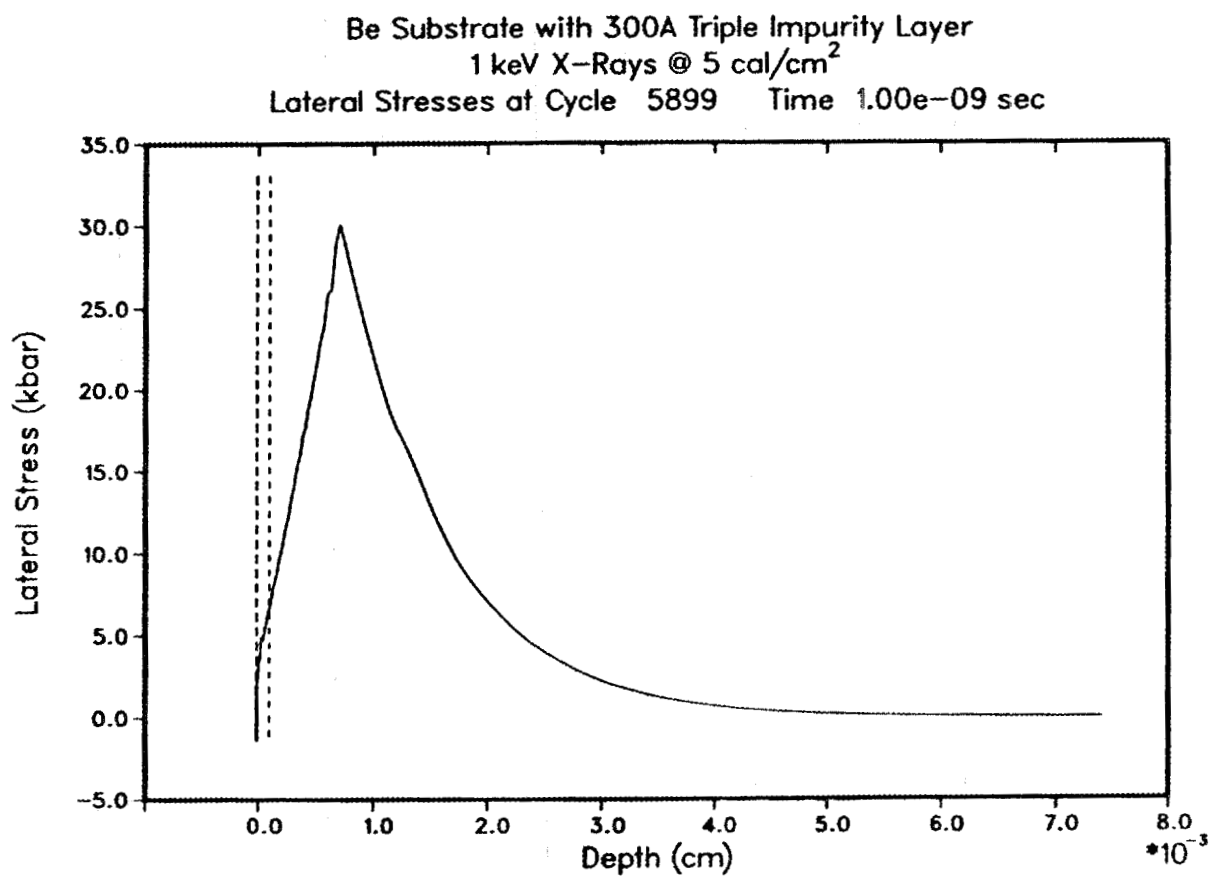


Figure 21. Lateral stress as a function of depth at 1.0 nanosecond for the 1 keV, 5 cal/cm<sup>2</sup> source incident upon the 300Å thick surface impurity layer with triple impurity concentrations.

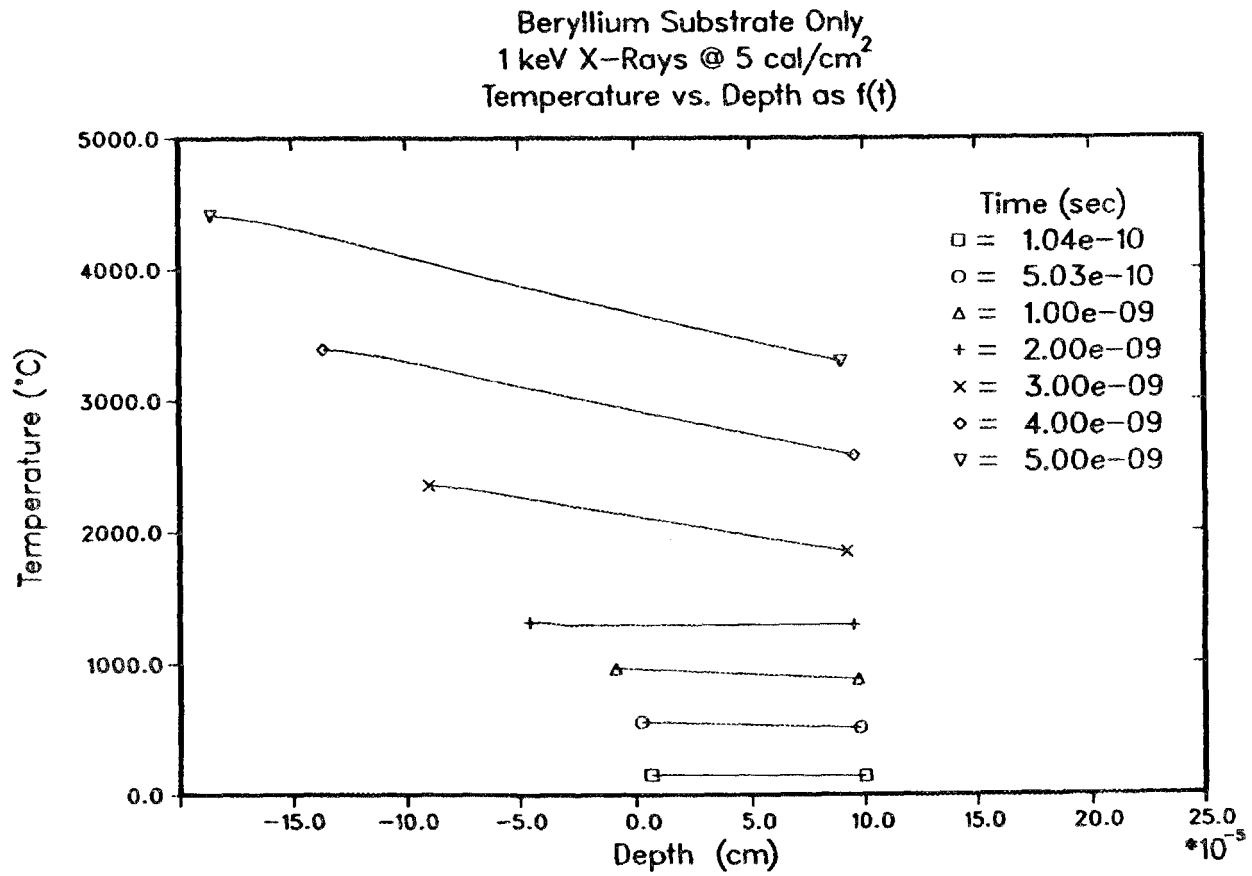


Figure 22. Temperature as a function of depth at specific times for the 1 keV, 5 cal/cm<sup>2</sup> source incident upon the beryllium substrate (no surface impurity layer).

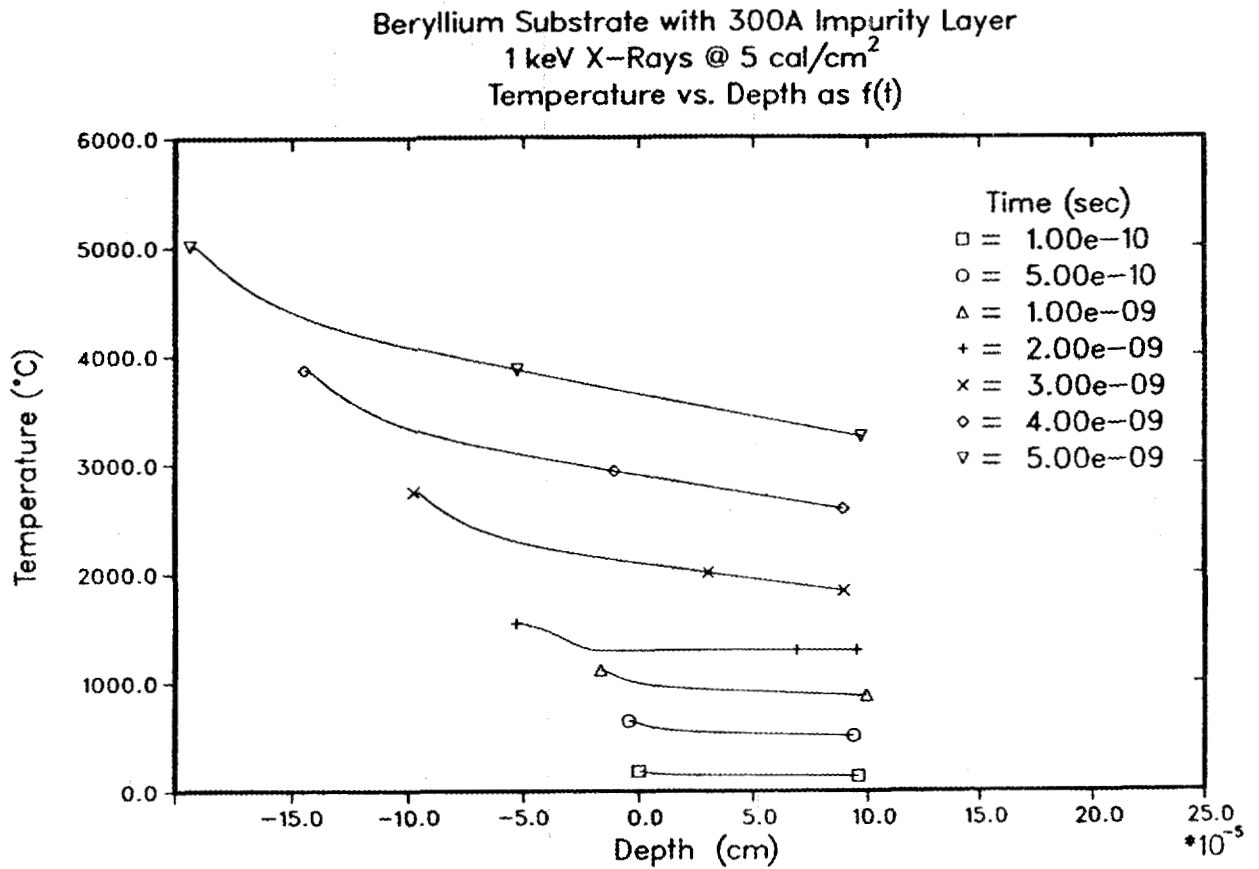


Figure 23. Temperature as a function of depth at specific times for the 1 keV, 5 cal/cm<sup>2</sup> source incident upon the 300Å thick surface impurity layer with the base impurity concentrations.

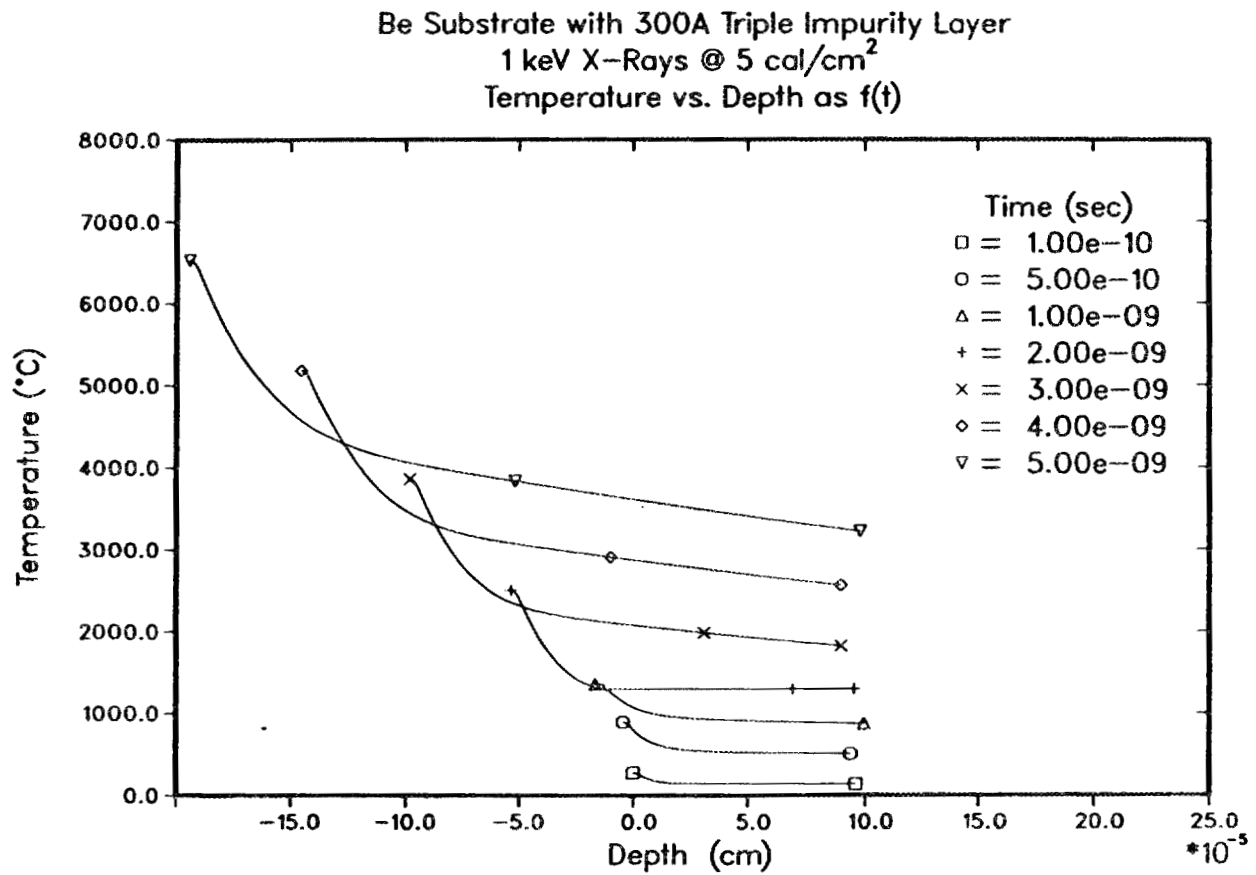


Figure 24. Temperature as a function of depth at specific times for the 1 keV, 5 cal/cm<sup>2</sup> source incident upon the 300Å thick surface impurity layer with triple impurity concentrations.

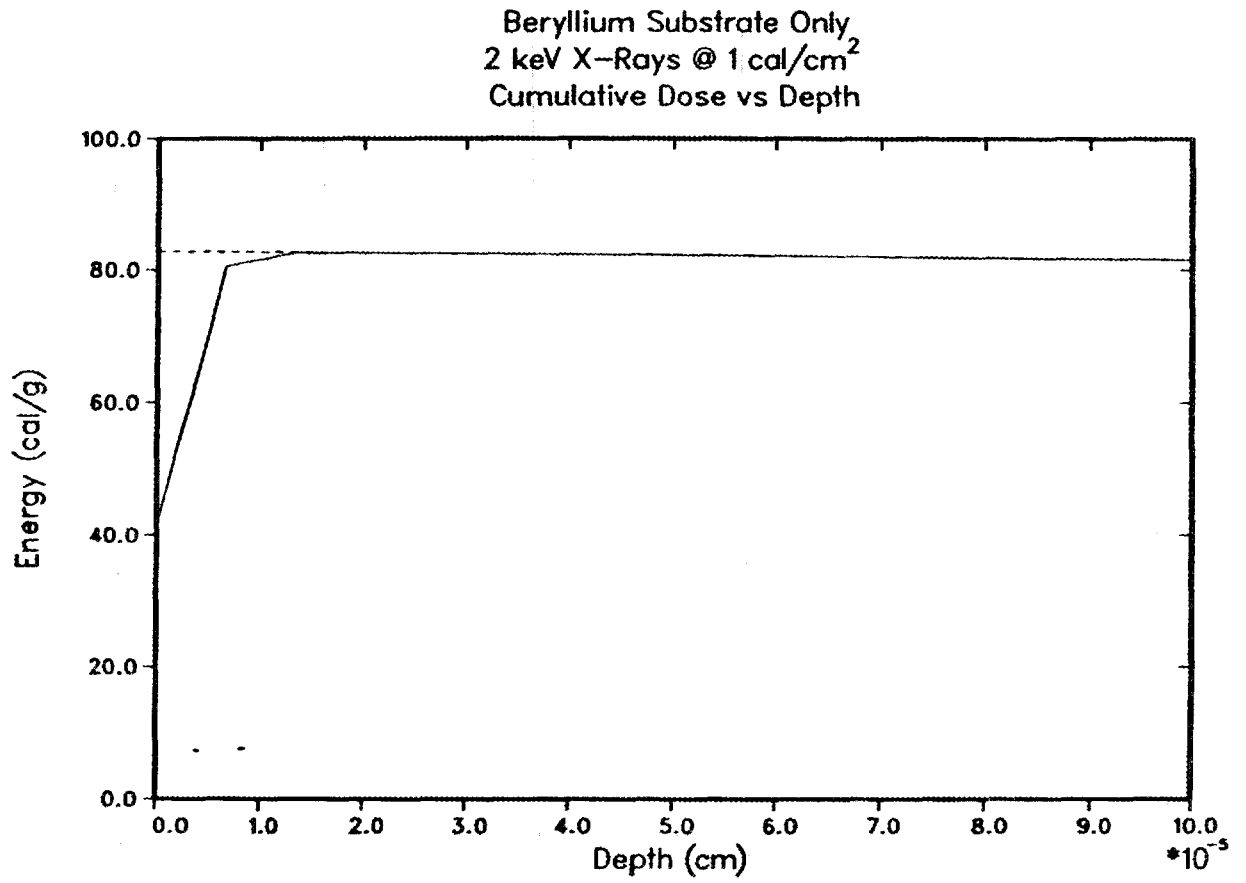


Figure 25. Energy deposited as a function of depth for the 2 keV, 1 cal/cm<sup>2</sup> source incident upon the beryllium substrate (no surface impurity layer).

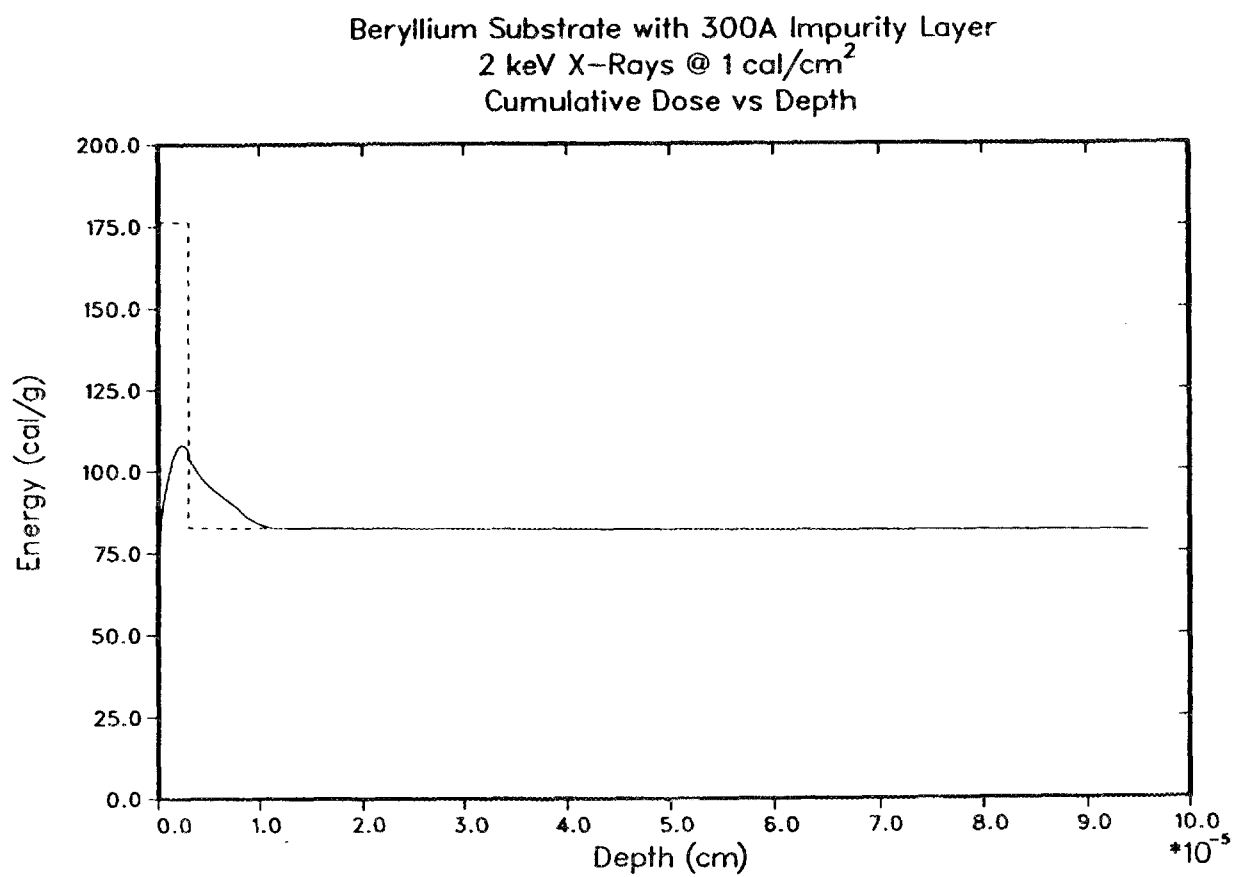


Figure 26. Energy deposited as a function of depth for the 2 keV, 1 cal/cm<sup>2</sup> source incident upon the 300Å thick surface impurity layer with the base impurity concentrations.

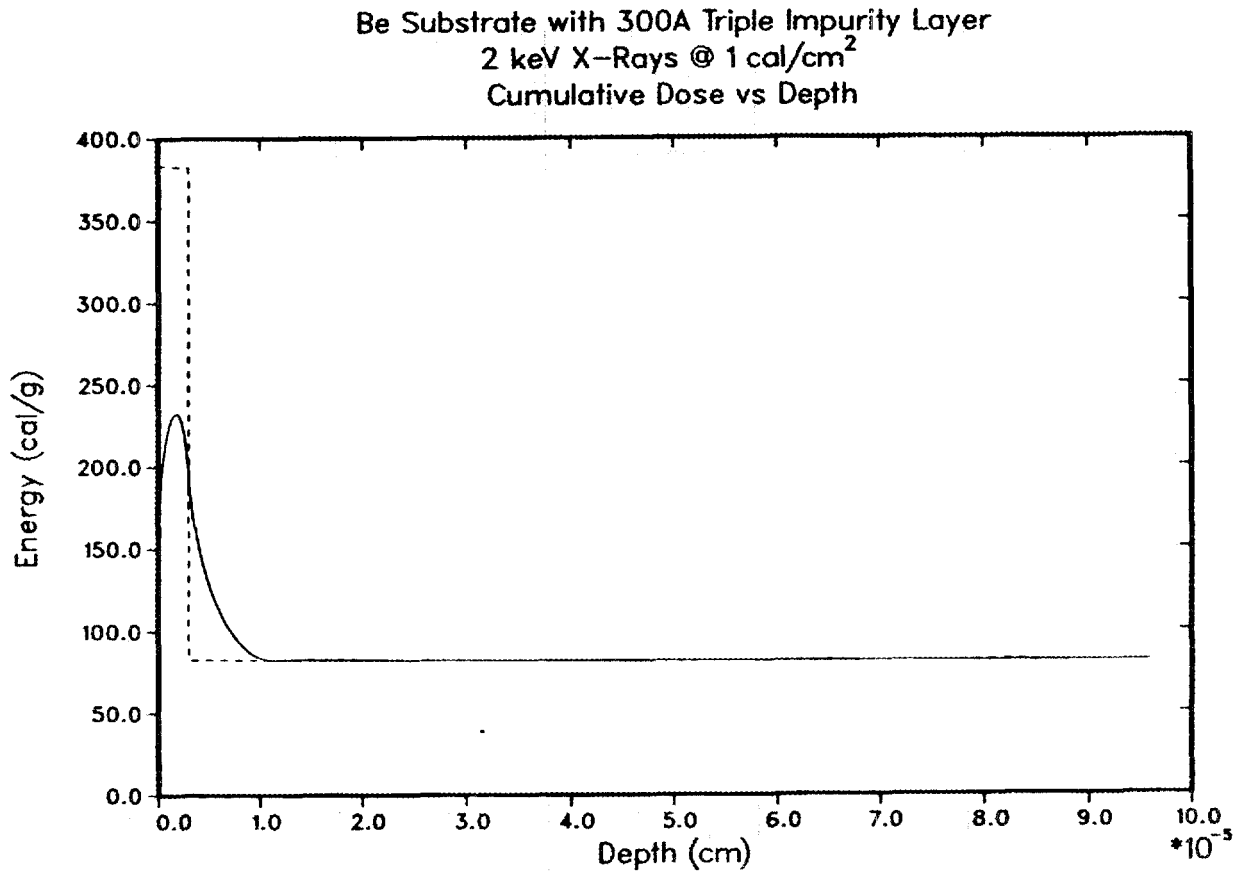


Figure 27. Energy deposited as a function of depth for the 2 keV, 1 cal/cm<sup>2</sup> source incident upon the 300Å thick surface impurity layer with triple impurity concentrations.

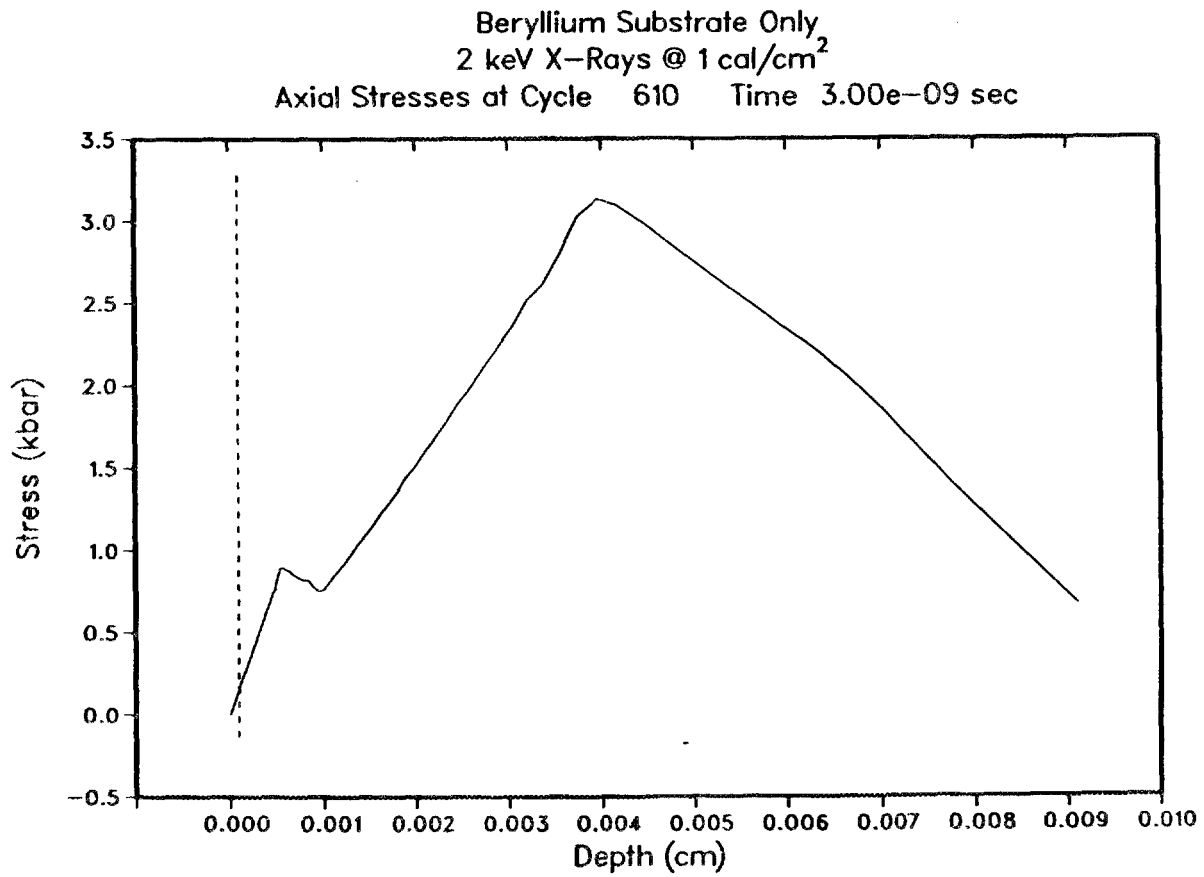


Figure 28. Axial stress as a function of depth at 3.0 nanoseconds for the 2 keV, 1 cal/cm<sup>2</sup> source incident upon the beryllium substrate (no surface impurity layer).

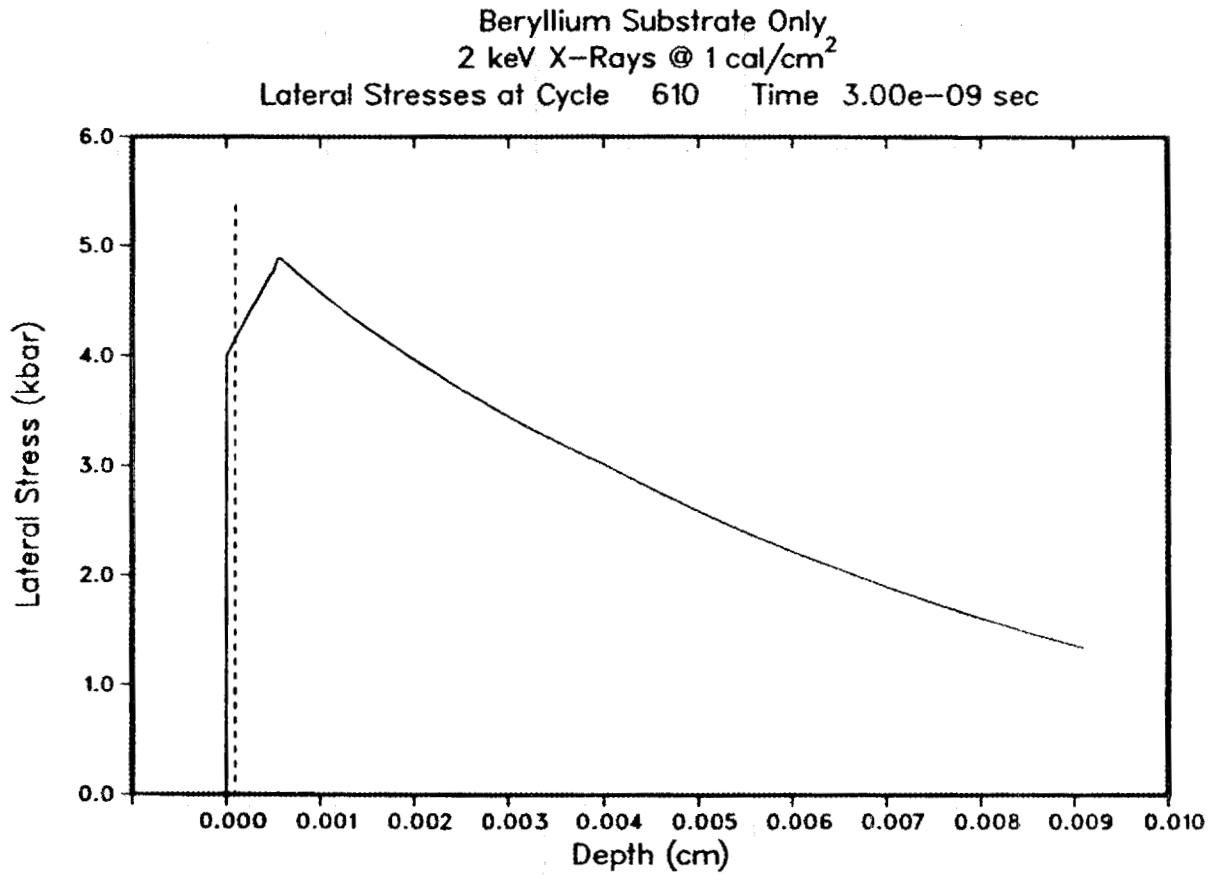


Figure 29. Lateral stress as a function of depth at 3.0 nanoseconds for the 2 keV, 1 cal/cm<sup>2</sup> source incident upon the beryllium substrate (no surface impurity layer).

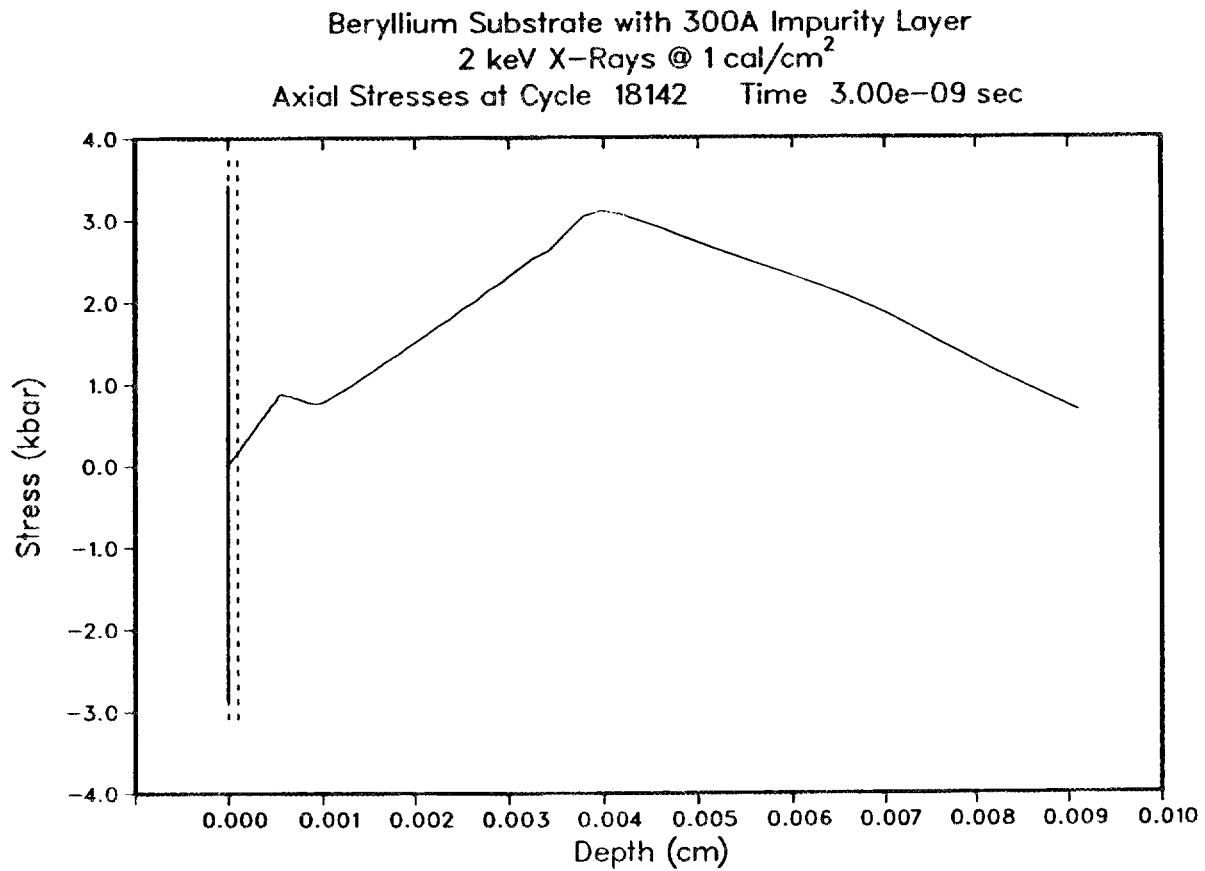


Figure 30. Axial stress as a function of depth at 3.0 nanoseconds for the 2 keV, 1 cal/cm<sup>2</sup> source incident upon the 300Å thick surface impurity layer with the base impurity concentrations.

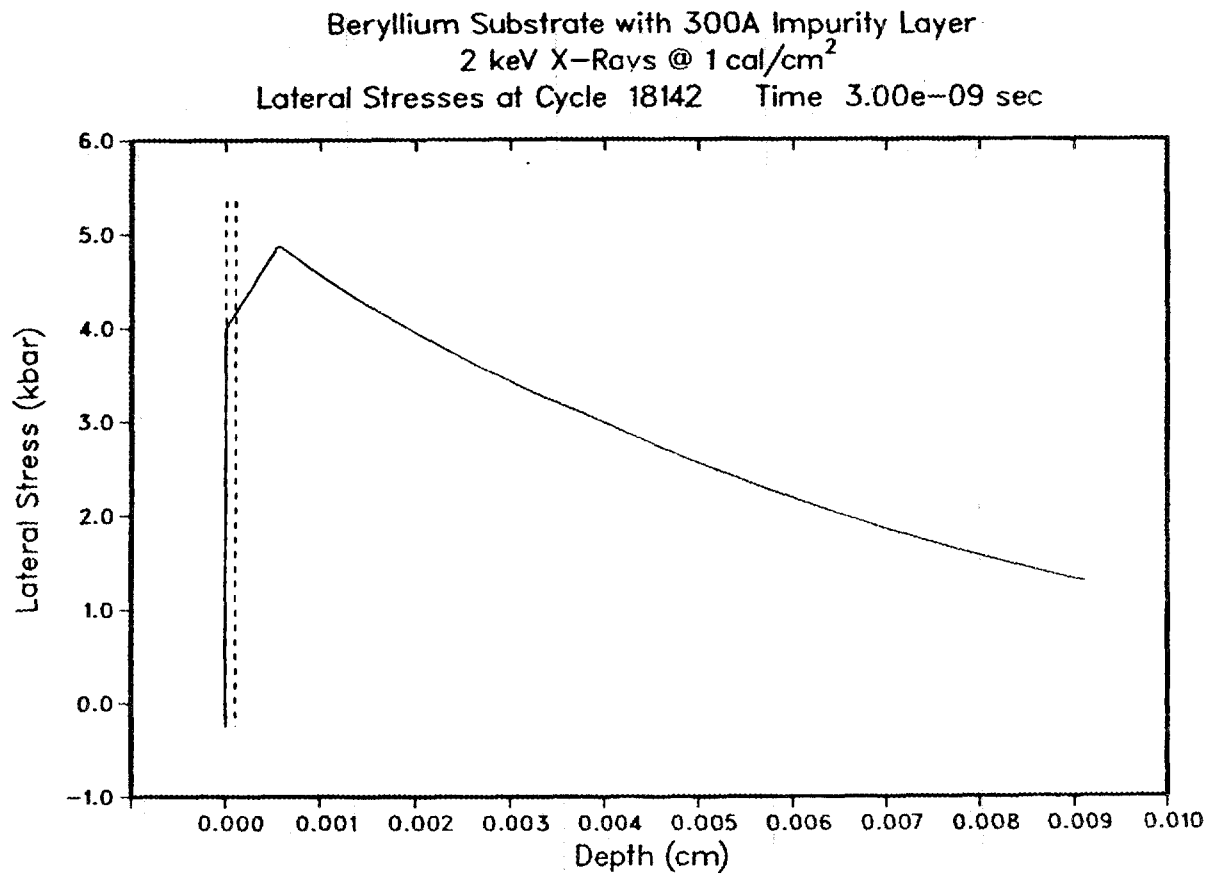


Figure 31. Lateral stress as a function of depth at 3.0 nanoseconds for the 2 keV, 1 cal/cm<sup>2</sup> source incident upon the 300Å thick surface impurity layer with the base impurity concentrations.

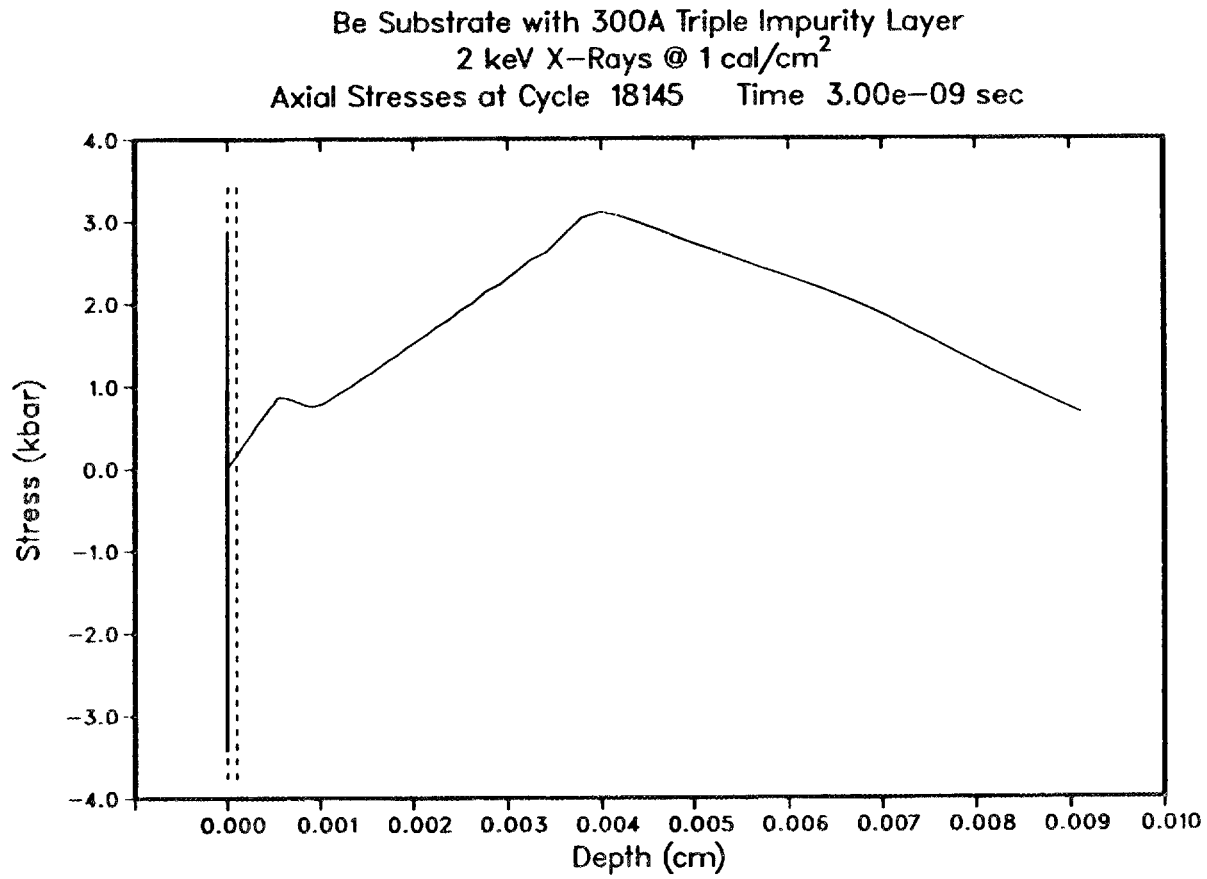


Figure 32. Axial stress as a function of depth at 3.0 nanoseconds for the 2 keV, 1 cal/cm<sup>2</sup> source incident upon the 300Å thick surface impurity layer with triple impurity concentrations.

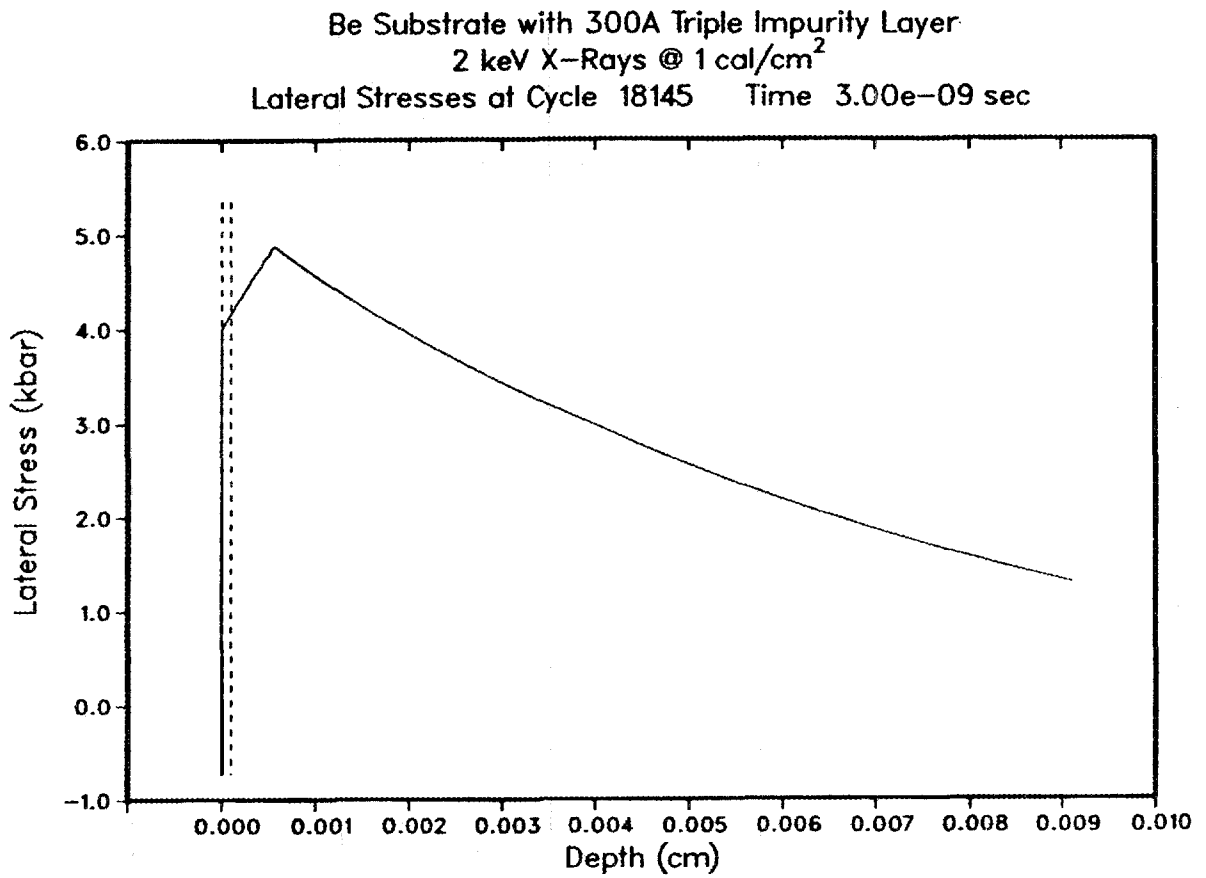


Figure 33. Lateral stress as a function of depth at 1.0 nanosecond for the keV,  $\text{cal/cm}^2$  source incident upon the 300Å thick surface impurity layer with triple impurity concentrations.

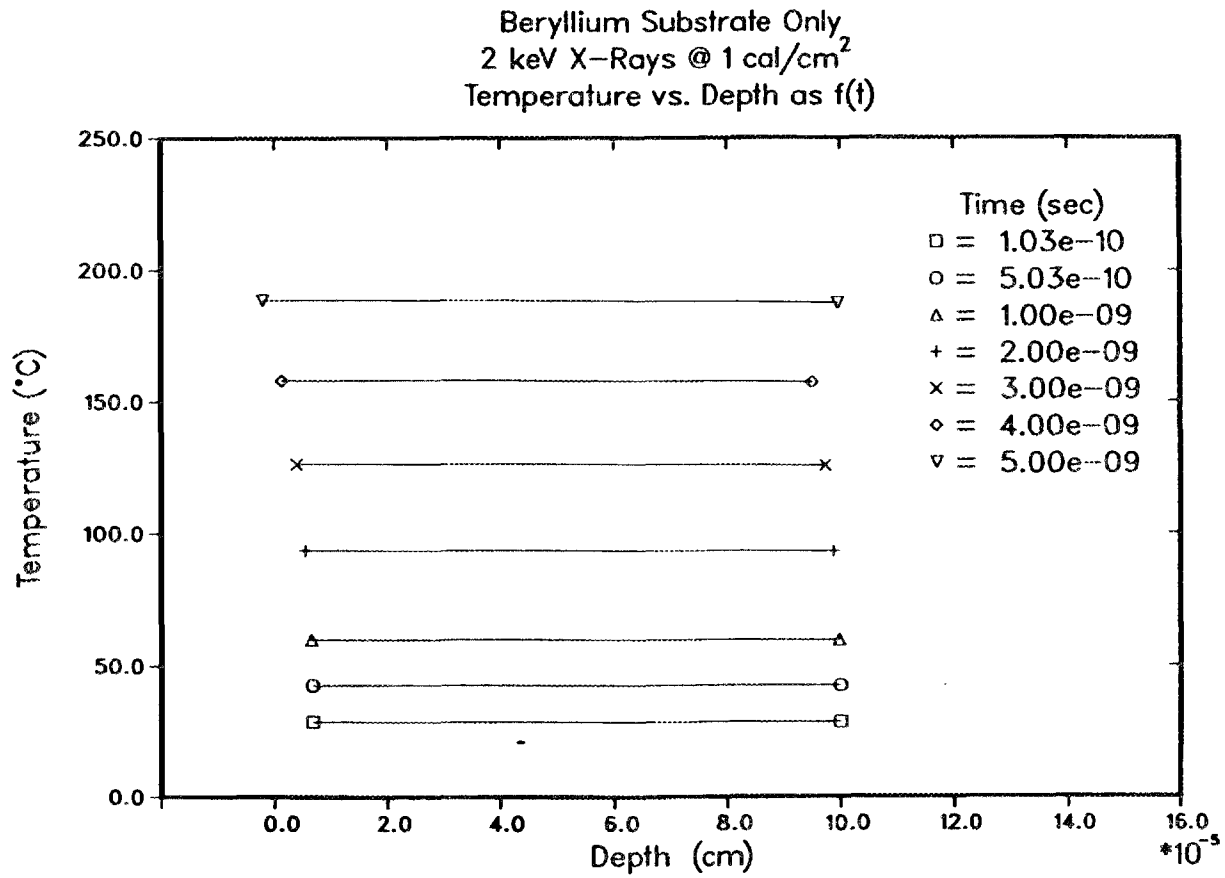


Figure 34. Temperature as a function of depth at specific times for the 2 keV, 1 cal/cm<sup>2</sup> source incident upon the beryllium substrate (no surface impurity layer).

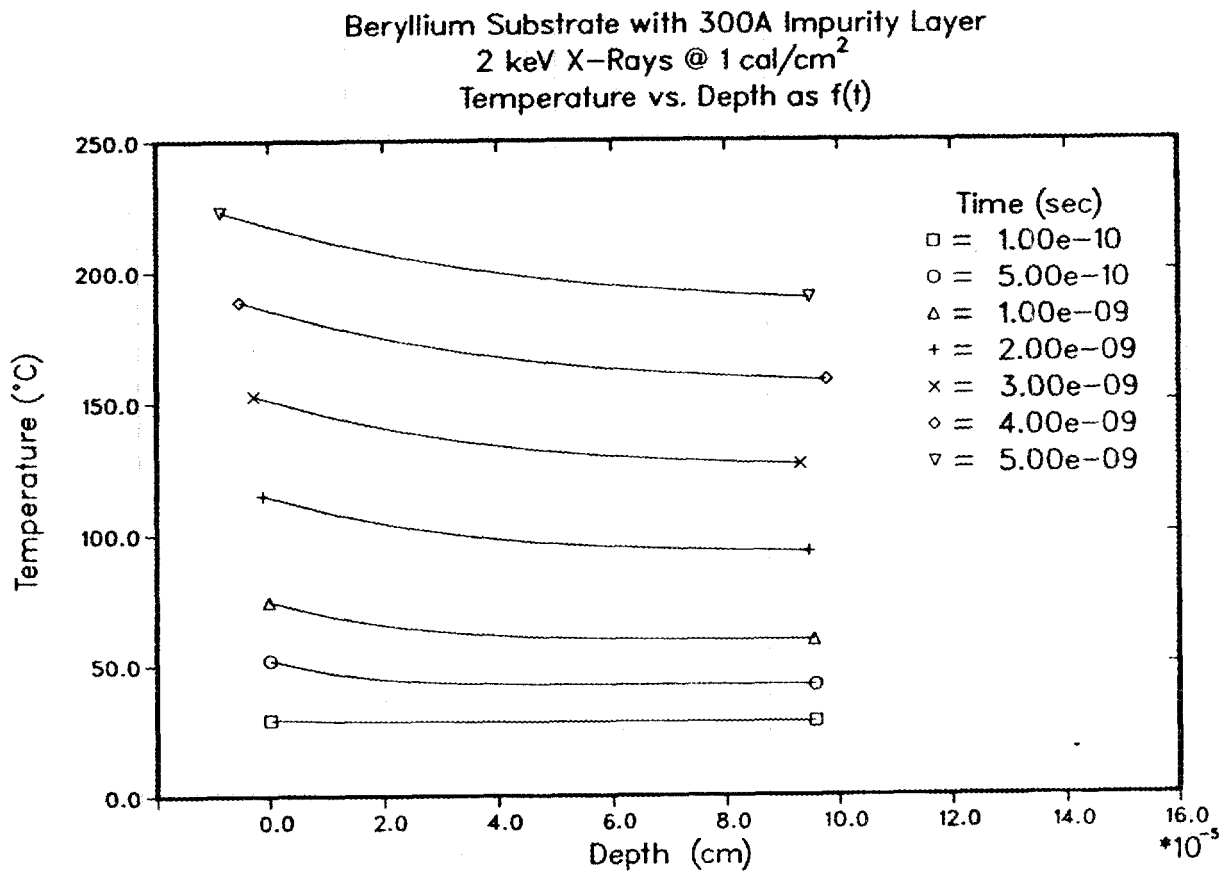


Figure 35. Temperature as a function of depth at specific times for the 2 keV, 1 cal/cm<sup>2</sup> source incident upon the 300Å thick surface impurity layer with the base impurity concentrations.

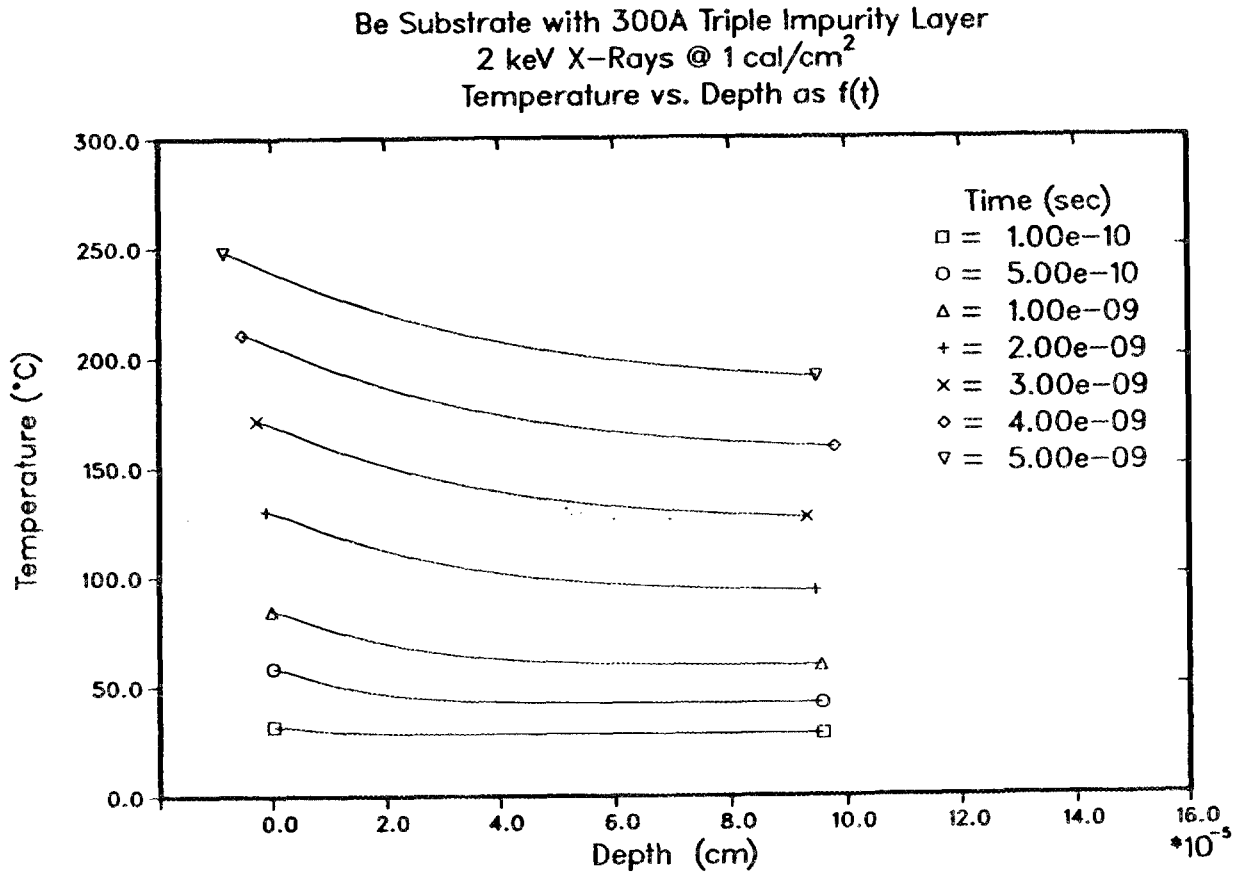


Figure 36. Temperature as a function of depth at specific times for the 2 keV, 1 cal/cm<sup>2</sup> source incident upon the 300Å thick surface impurity layer with triple impurity concentrations.

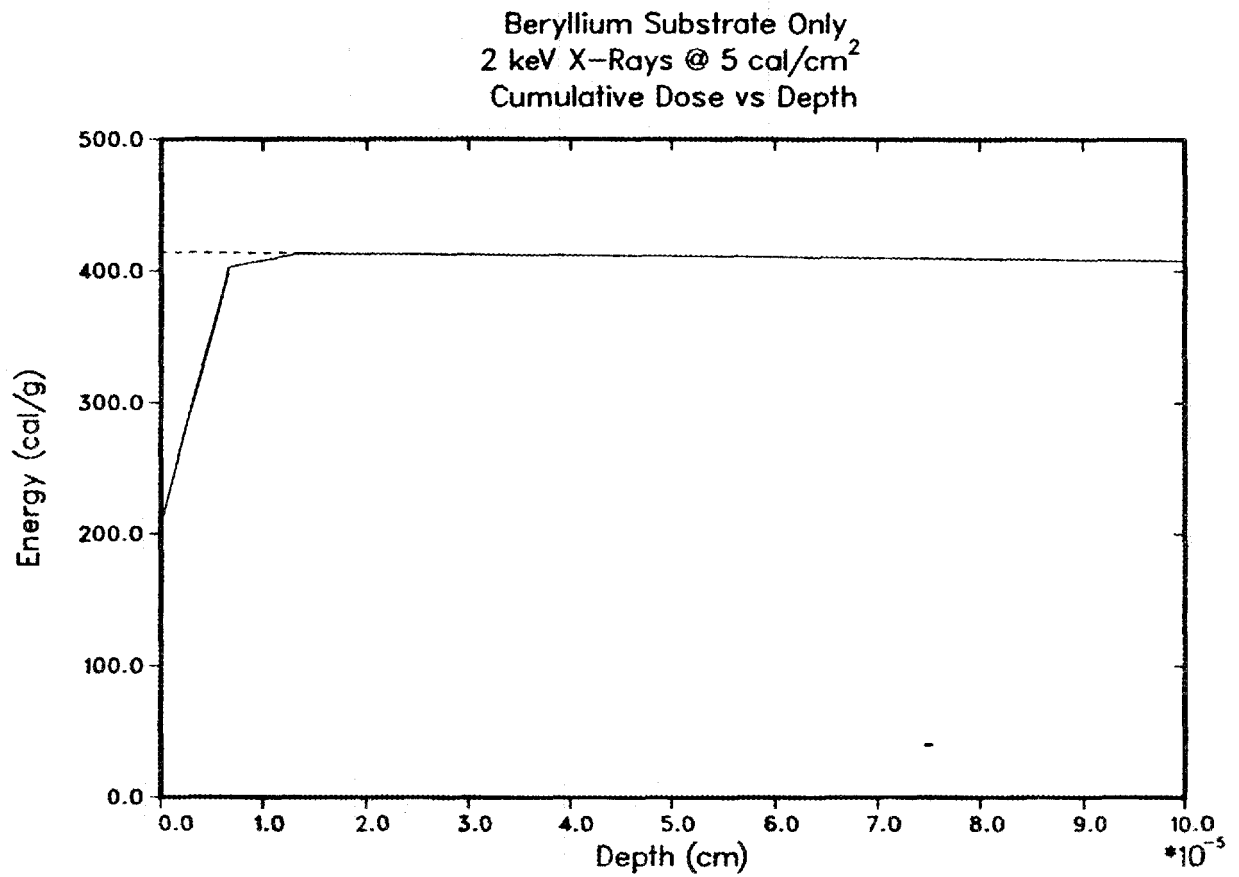


Figure 37. Energy deposited as a function of depth for the 2 keV, 5 cal/cm<sup>2</sup> source incident upon the beryllium substrate (no surface impurity layer).

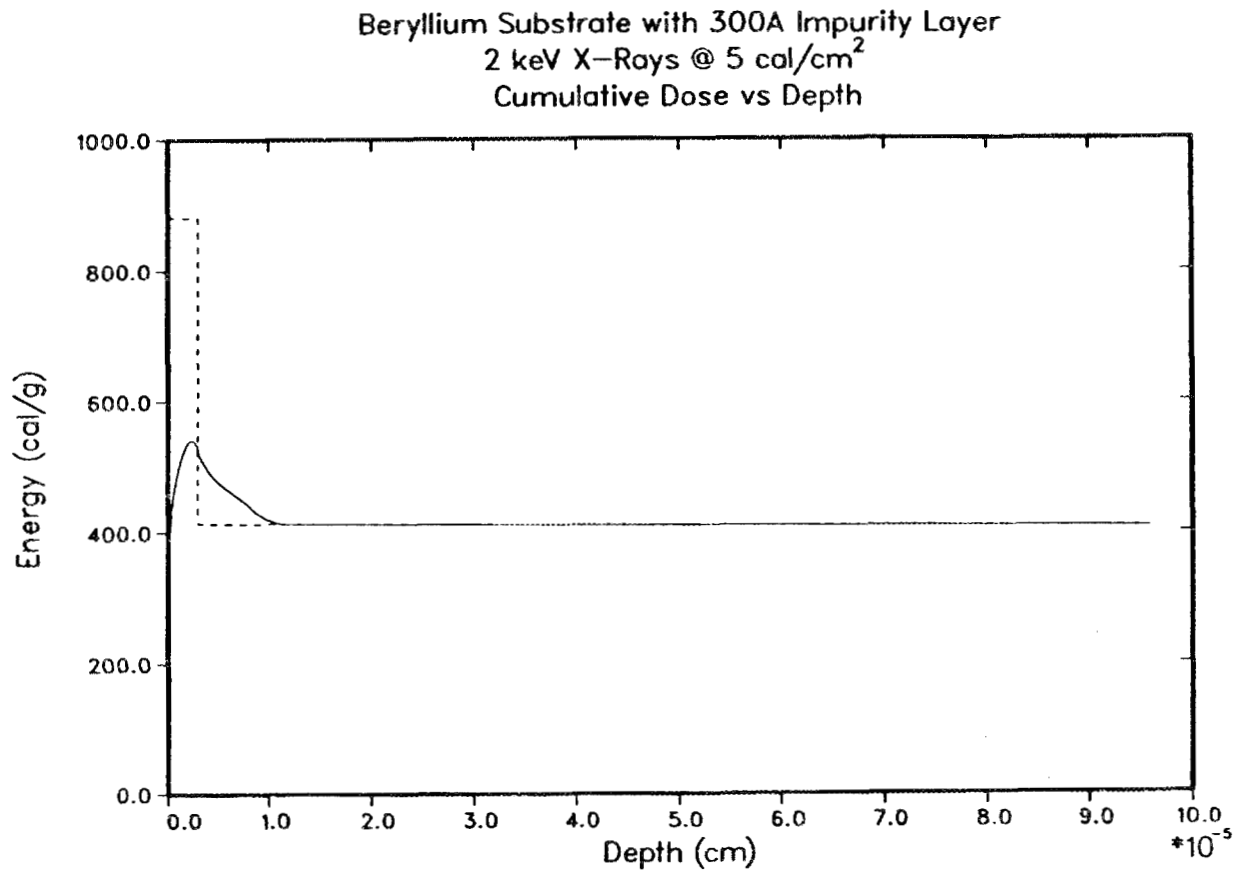


Figure 38. Energy deposited as a function of depth for the 2 keV, 5 cal/cm<sup>2</sup> source incident upon the 300Å thick surface impurity layer with the base impurity concentrations.

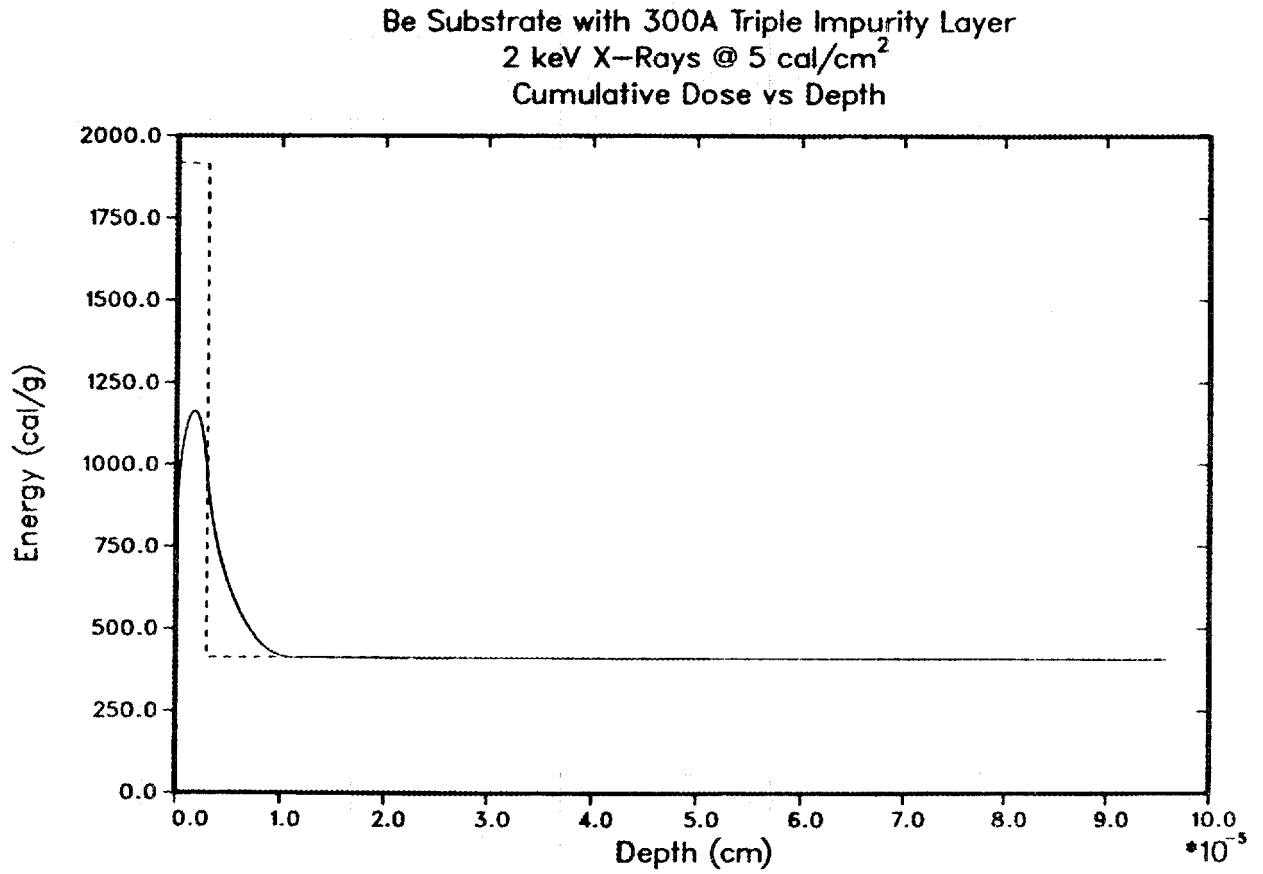


Figure 39. Energy deposited as a function of depth for the 2 keV, 5 cal/cm<sup>2</sup> source incident upon the 300Å thick surface impurity layer with triple impurity concentrations.

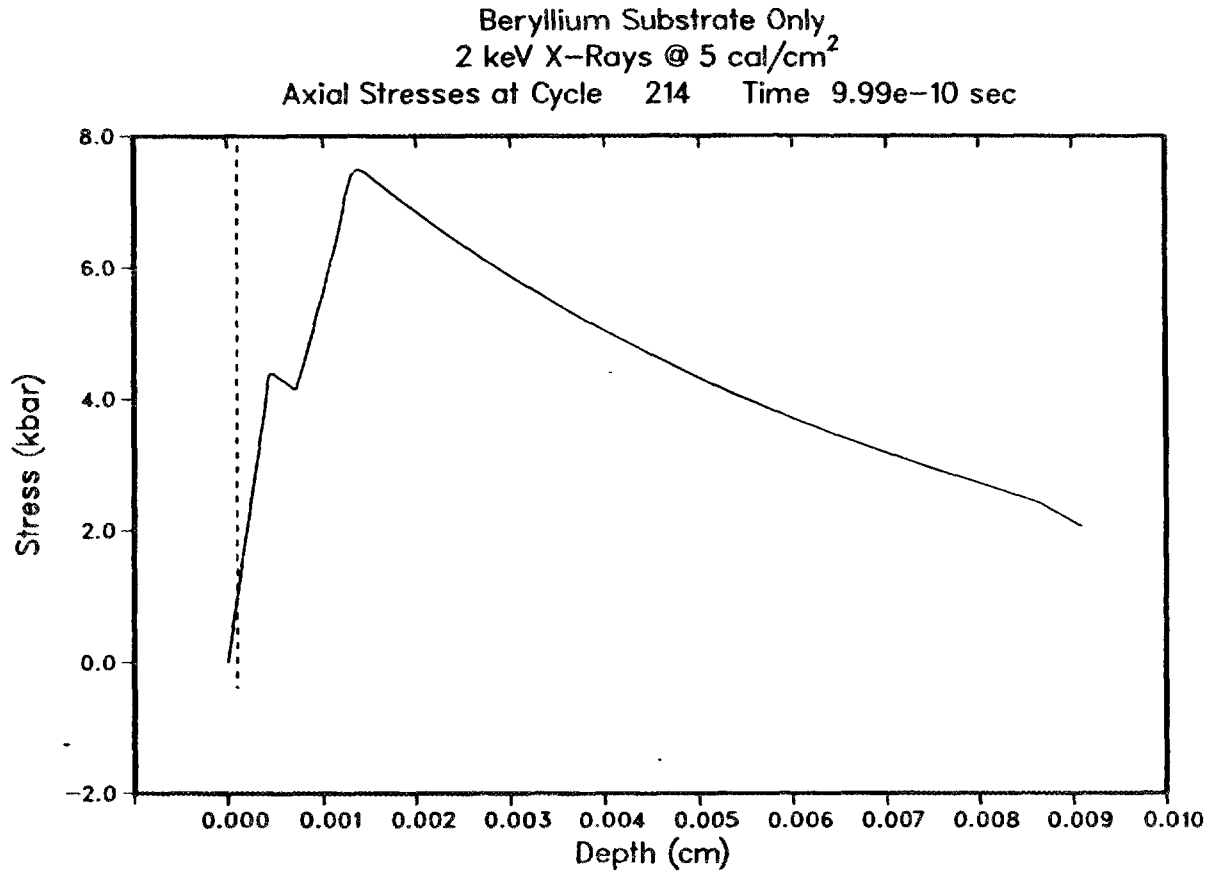


Figure 40. Axial stress as a function of depth at 1.0 nanosecond for the 2 keV, 5 cal/cm<sup>2</sup> source incident upon the beryllium substrate (no surface impurity layer).

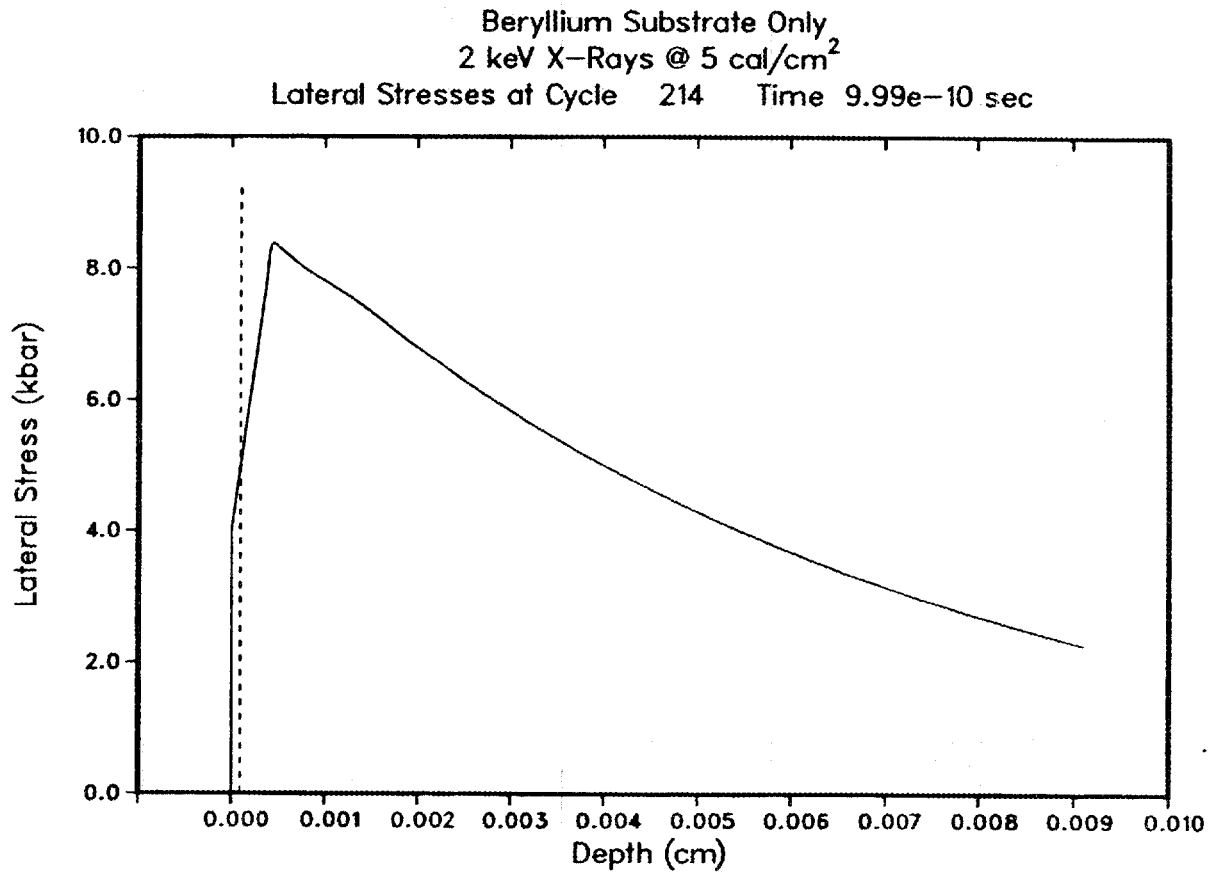


Figure 41. Lateral stress as a function of depth at 1.0 nanosecond for the 2 keV, 5 cal/cm<sup>2</sup> source incident upon the beryllium substrate (no surface impurity layer).

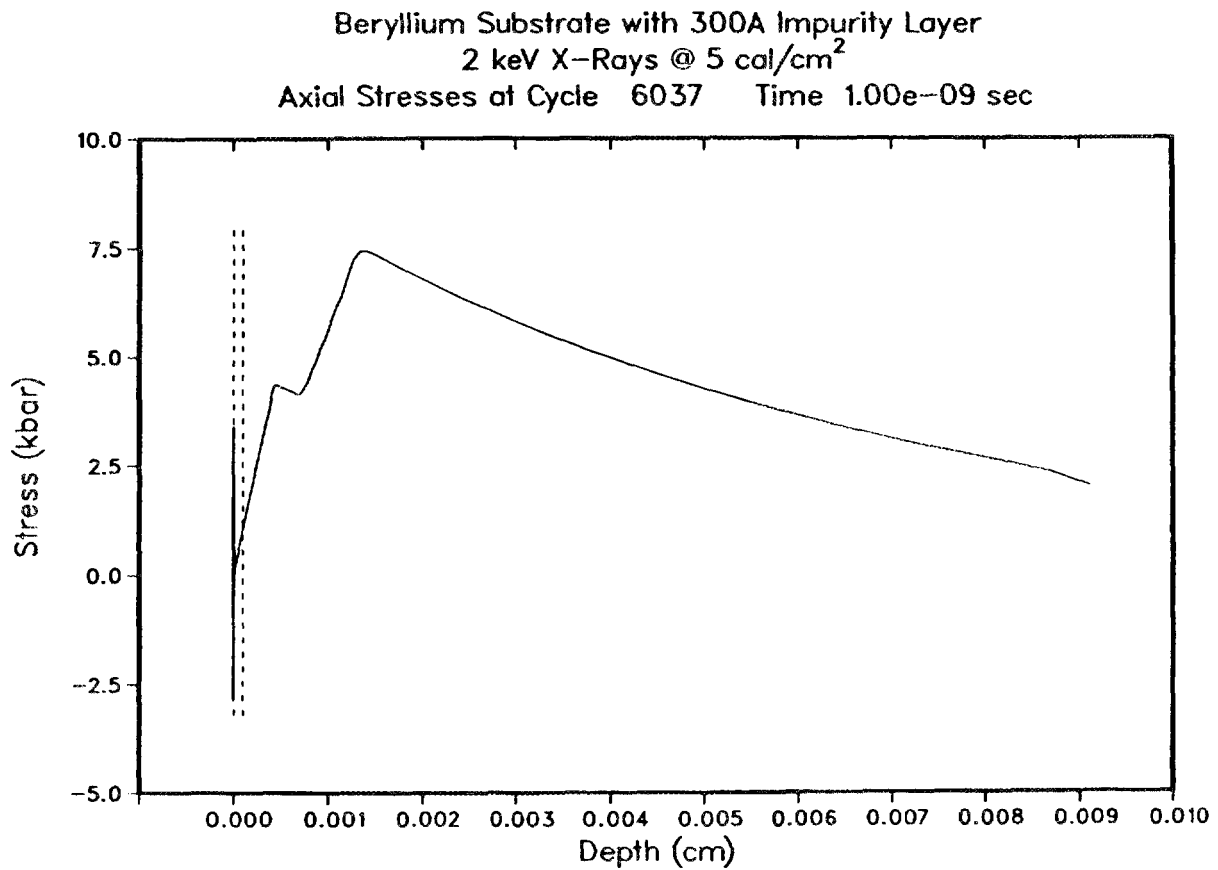


Figure 42. Axial stress as a function of depth at 1.0 nanosecond for the 2 keV, 5 cal/cm<sup>2</sup> source incident upon the 300Å thick surface impurity layer with the base impurity concentrations.

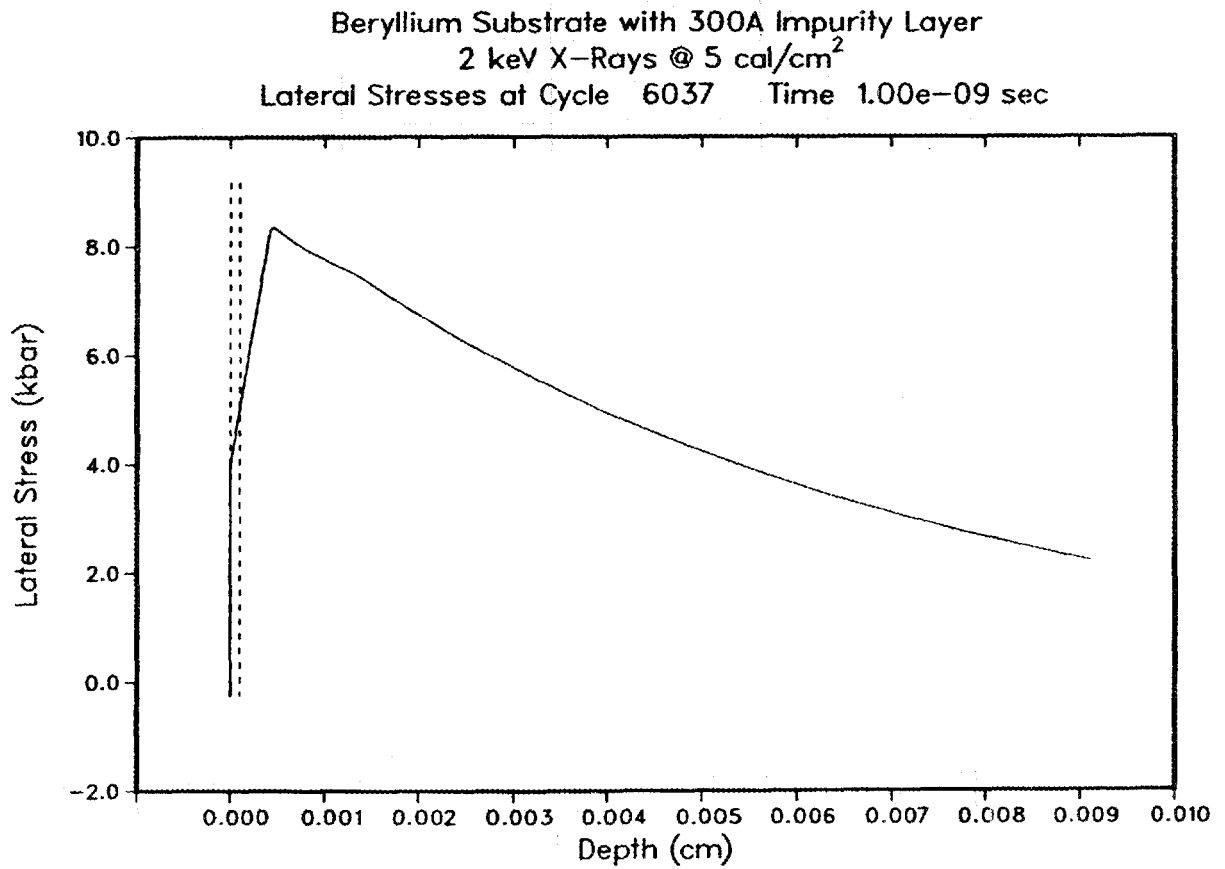


Figure 43. Lateral stress as a function of depth at 1.0 nanosecond for the 2 keV, 5 cal/cm<sup>2</sup> source incident upon the 300Å thick surface impurity layer with the base impurity concentrations.

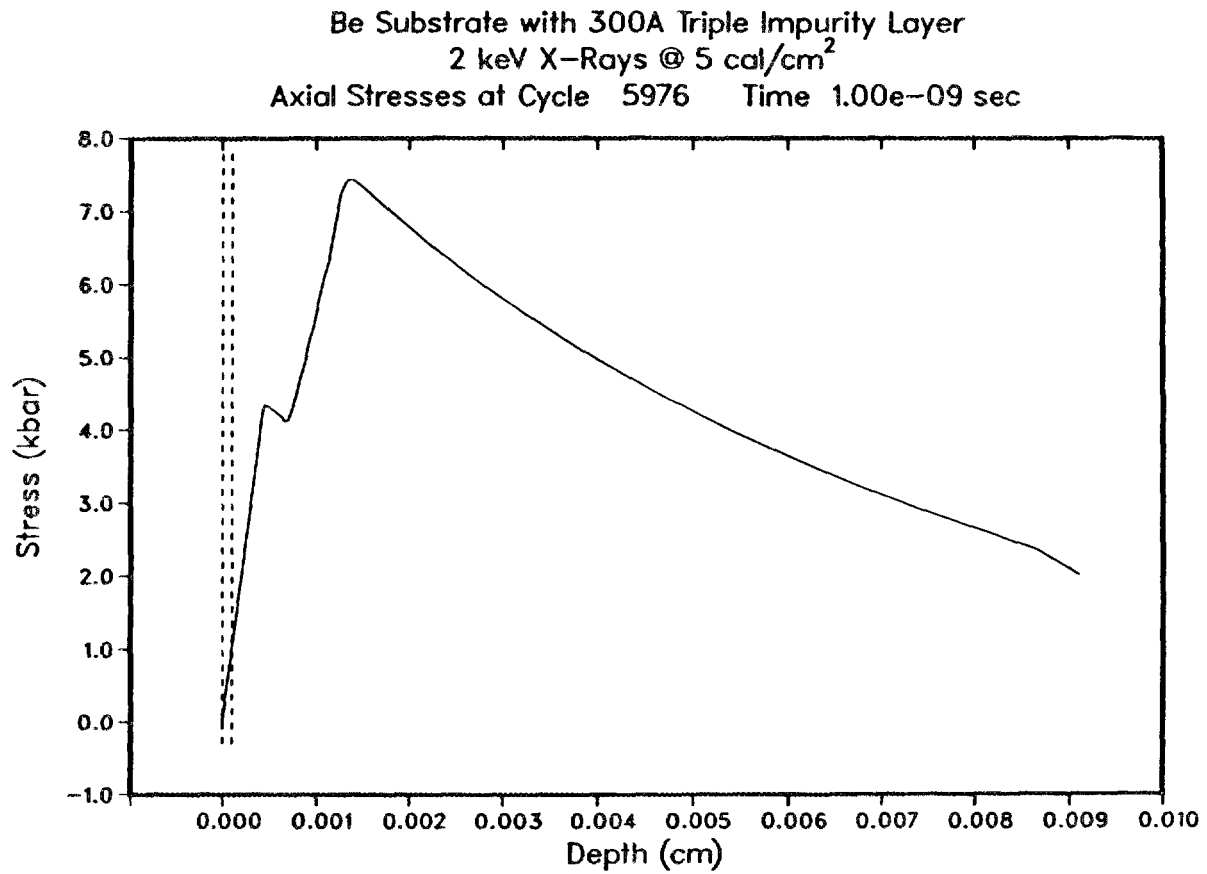


Figure 44. Axial stress as a function of depth at 1.0 nanosecond for the 2 keV, 5 cal/cm<sup>2</sup> source incident upon the 300Å thick surface impurity layer with triple impurity concentrations.

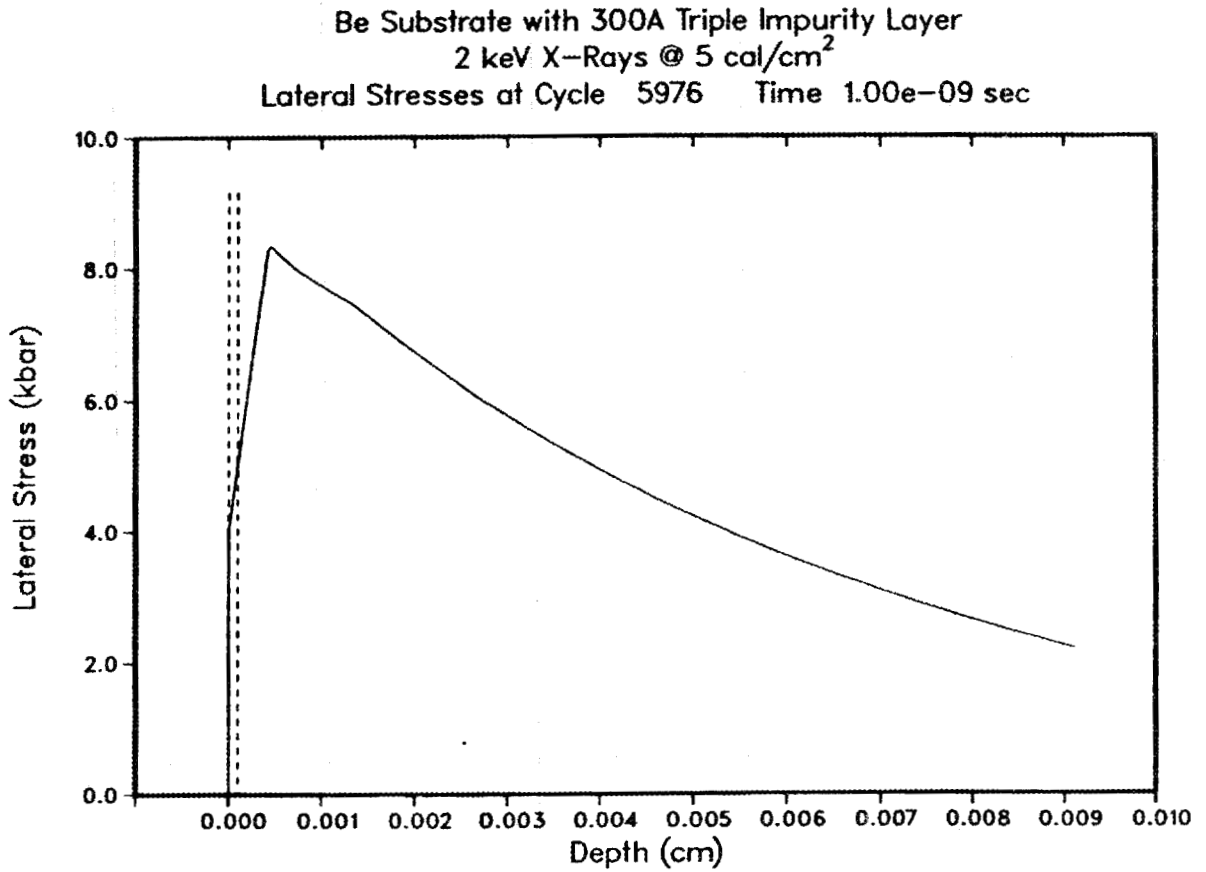


Figure 45. Lateral stress as a function of depth at 1.0 nanosecond for the 2 keV, 5 cal/cm<sup>2</sup> source incident upon the 300Å thick surface impurity layer with triple impurity concentrations.

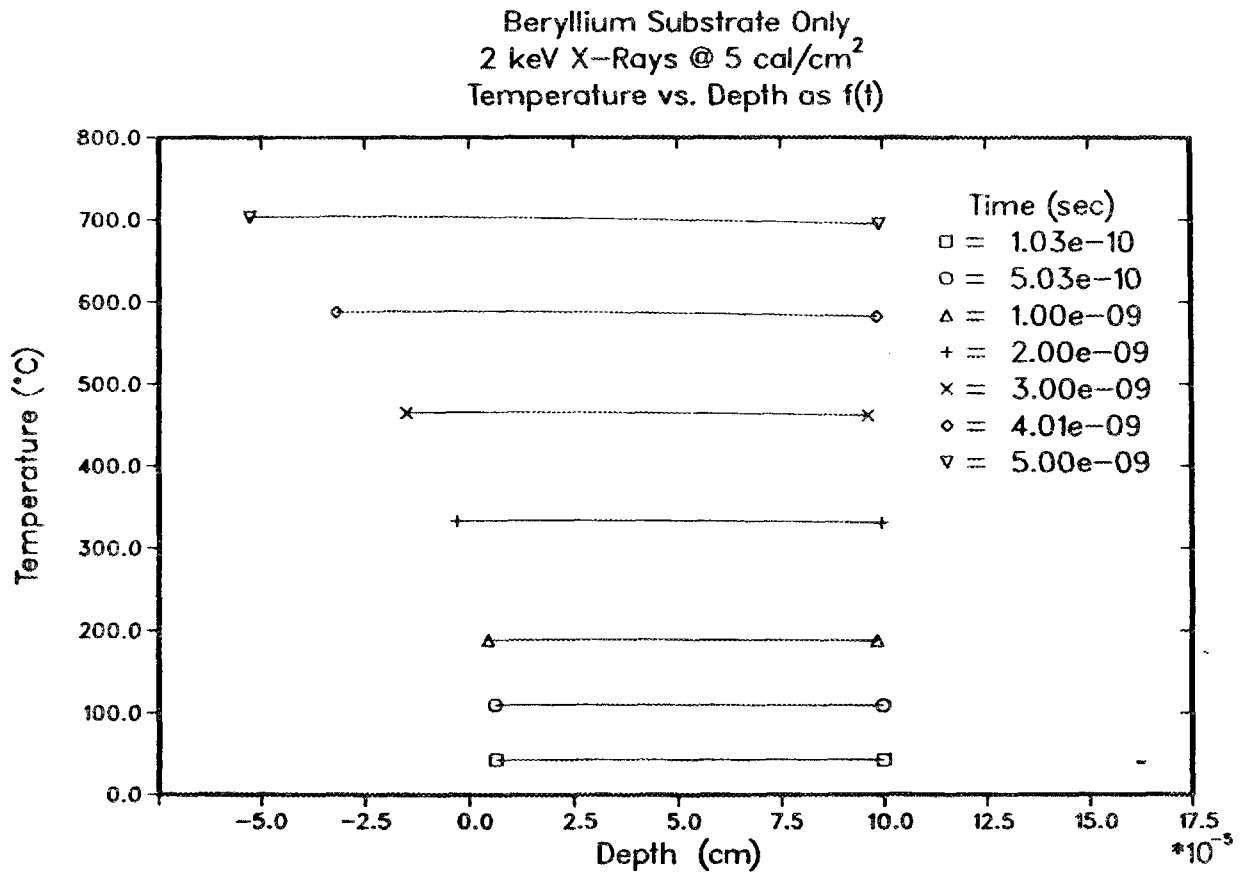


Figure 46. Temperature as a function of depth at specific times for the 2 keV, 5 cal/cm<sup>2</sup> source incident upon the beryllium substrate (no surface impurity layer).

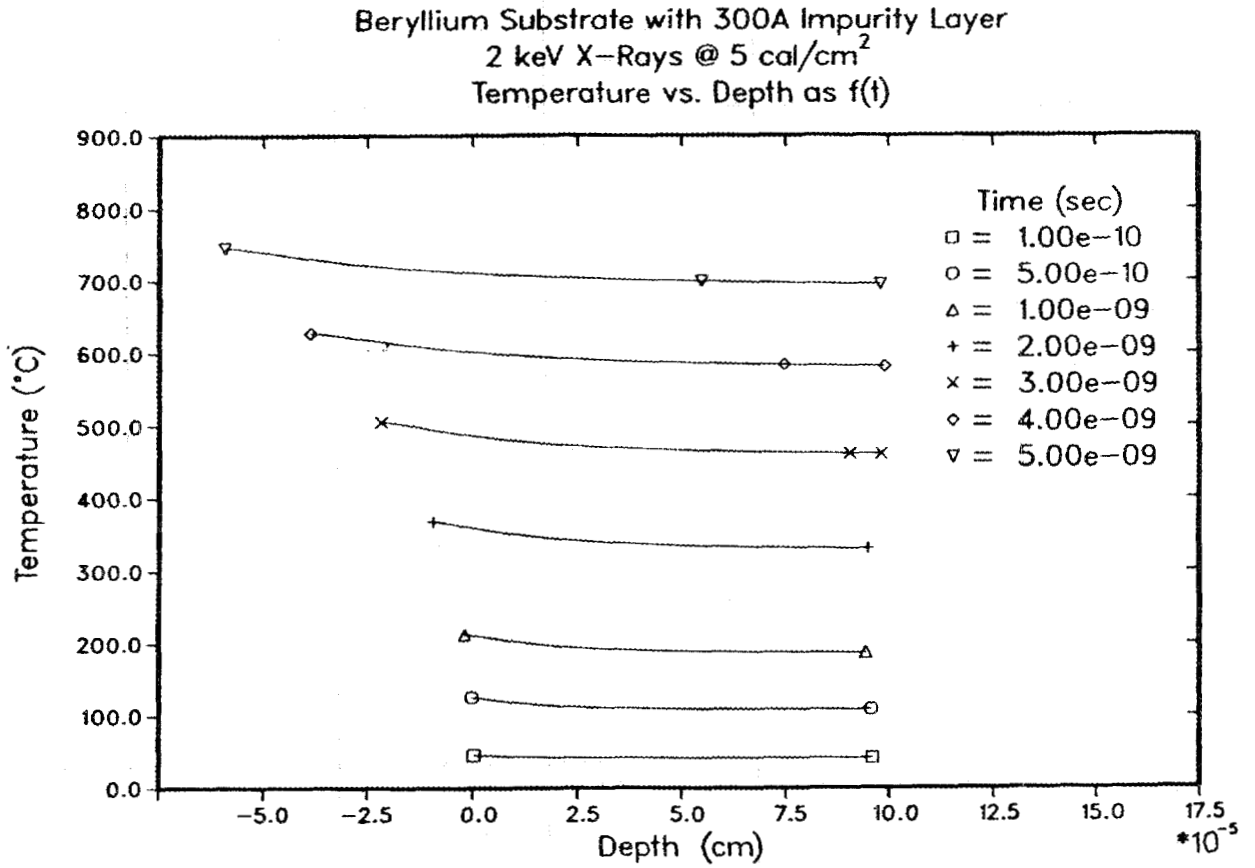


Figure 47. Temperature as a function of depth at specific times for the 2 keV, 5 cal/cm<sup>2</sup> source incident upon the 300Å thick surface impurity layer with the base impurity concentrations.

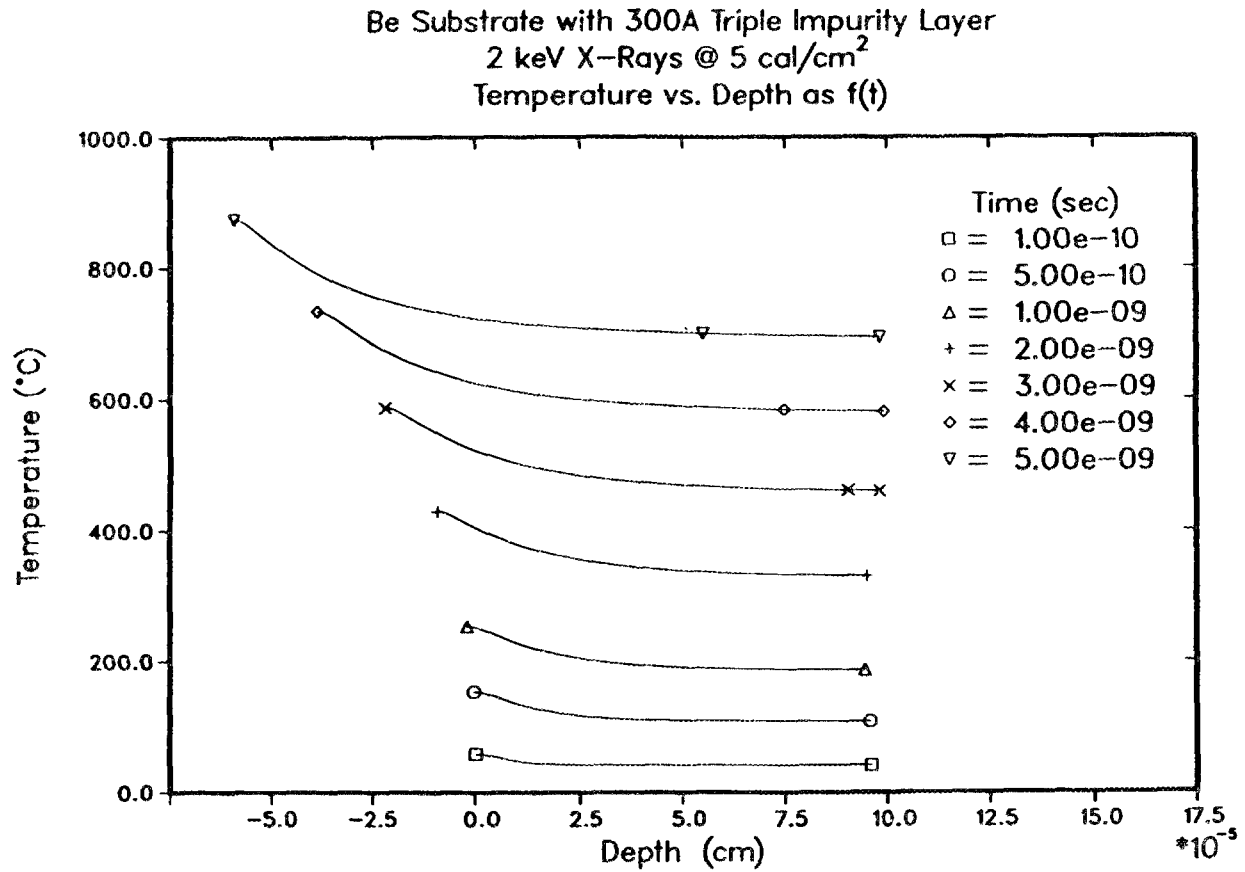


Figure 48. Temperature as a function of depth at specific times for the 2 keV, 5 cal/cm<sup>2</sup> source incident upon the 300Å thick surface impurity layer with triple impurity concentrations.

Appendix A.  
PUFF-TFT Sample Input

```

Be Substrate with 300A Triple Impurity Layer
1 keV Blackbody 1 cal/cm&eh0.7)2&exhx)
1 3 -2 6 0 0 0 0 2 0 100040000 -1 0 0 0
1 40000 1.000e+00 5.000e-09 1.000e-13 0. 00000 0 0 0 01 1002
0 0 6 0
1 0.50000 1 1.00000
1.000e-10 5.000e-10 1.000e-09 2.000e-09 3.000e-09 4.000e-09
1.000e-10 5.000e-10 1.000e-09 2.000e-09 3.000e-09 4.000e-09
0. 1.000e-04
be imp 3.000e-06 1 0 0 0 1 0 0 0.0-6.000e+09 0.
8.800e+02 0. 0. 0. 0. 0. 0. 0.
4.000e+09 1.505e+12 0. 1.329e-03 0.
0. 0. 0. 0. 0.
4.501e-01 4.915e-04-1.469e-07 5.850e-01 3.240e+02 5.570e-01 7.816e+03
4.402e-01-4.394e-04 1.588e-07 1.240e-01

be imp 11 1-2.000e+00 0. 0. 1.204e+03-2.000e+00 1.204e+03
4 5.374e-01 6 7.290e-02 8 3.039e-01 9 2.880e-0213 1.020e-0214 1.080e-02
15 6.900e-0316 7.200e-0317 5.400e-0324 1.170e-0229 4.800e-03
1.848e+00 1.147e+12 1.893e+12 3.550e+11 1.450e+00 2.500e-01 0.
beryllium 1.000e-04 1 0 0 0 1 0 0 0.0-6.000e+09 0.
8.800e+02 0. 0. 0. 0. 0. 0. 0.
4.000e+09 1.505e+12 0. 1.329e-03 0.
0. 0. 0. 0. 0.
4.501e-01 4.915e-04-1.469e-07 5.850e-01 3.240e+02 5.570e-01 7.816e+03
4.402e-01-4.394e-04 1.588e-07 1.240e-01

beryllium 4 1-2.000e+00 0. 0. 1.204e+03-2.000e+00 1.204e+03
4 9.928e-01 8 3.500e-0313 3.000e-0326 6.000e-04
1.848e+00 1.147e+12 1.893e+12 3.550e+11 1.450e+00 2.500e-01 0.
beryllium 1.000e-02 1 0 0 0 1 0 0 0.0-6.000e+09 0.
8.800e+02 0. 0. 0. 0. 0. 0. 0.
4.000e+09 1.505e+12 0. 1.329e-03 0.
0. 0. 0. 0. 0.
4.501e-01 4.915e-04-1.469e-07 5.850e-01 3.240e+02 5.570e-01 7.816e+03
4.402e-01-4.394e-04 1.588e-07 1.240e-01

beryllium 4 1-2.000e+00 0. 0. 1.204e+03-2.000e+00 1.204e+03
4 9.928e-01 8 3.500e-0313 3.000e-0326 6.000e-04
1.848e+00 1.147e+12 1.893e+12 3.550e+11 1.450e+00 2.500e-01 0.
3 1.000e+00 0. 5.000e-09 0 1.000e+00 0. 0 0

```

## REFERENCES

1. A. J. Watts, C. Breen, S. Sauer, and F. Smith, "Thin Film Transport (PUFF-TFT) Computer Code Development," AFWL-TR-88-66, Parts 1 and 2, Air Force Weapons Laboratory, Kirtland AFB, NM, June 1988.
2. R. Cecil, C. D. Newlander, and R. T. Scannon, "PUFF74 - A Material Response Computer Code," AFWL-TR-76-43, Volumes I and II, Air Force Weapons Laboratory, Kirtland AFB, NM, January 1977.
3. W. H. Childs, "Thermophysical Properties of Selected Space-Related Materials," TOR-0081(6435-02)-1, Volume I, Aerospace Corporation, Los Angeles, CA, February 1981.
4. W. H. Childs, "Thermophysical Properties of Selected Space-Related Materials," TOR-0086(6435-02)-1, Volume II, Aerospace Corporation, Los Angeles, CA, February 1986.
5. M. H. Rice, "PUFF74 EOS Compilation," AFWL-TR-80-21, Air Force Weapons Laboratory, Kirtland AFB, NM, August 1980.
6. S. Sauer, Private Communication, 31 March 1988.

## INTERNAL DISTRIBUTION

- |                         |   |
|-------------------------|---|
| 1. M. A. Akerman        | 27. J. R. Merriman                      |
| 2. R. G. Alsmiller, Jr. | 28. W. L. Roberts                       |
| 3. B. R. Appleton       | 29. R. W. Roussin                       |
| 4. D. E. Bartine        | 30-34. R. T. Santoro                    |
| 5. J. M. Barnes         | 35-39. M. S. Smith                      |
| 6. T. J. Burns          | 40. D. G. Thomas                        |
| 7. R. M. Davis          | 41. R. C. Ward                          |
| 8. J. B. Dooley         | 42. C. R. Weisbin                       |
| 9. J. D. Drischler      | 43. J. M. Williams                      |
| 10-14. T. A. Gabriel    | 44. EPMD Reports Office                 |
| 15. C. M. Haaland       | 45-46. Laboratory Records<br>Department |
| 16. E. B. Harris        | 47. Laboratory Records,<br>ORNL-RC      |
| 17. D. T. Ingersoll     | 48. Document Reference<br>Section       |
| 18. J. O. Johnson       | 49. Central Research Library            |
| 19. R. A. Lillie        | 50. ORNL Patent Section                 |
| 20. F. C. Maienschein   |   |
| 21-25. S. McNeany       |   |
| 26. J. R. McNeely       |   |

## EXTERNAL DISTRIBUTION

51. Dr. Charles Aeby, AFWL/NTC, Air Force Weapons Laboratory, Kirtland Air Force Base, New Mexico 87117-6008
52. Lt Dale Atkinson, AFWL/NTCA, Air Force Weapons Laboratory, Kirtland Air Force Base, New Mexico 87117-6008
53. Richard Bradshaw, U.S. Army Strategic Defense Command, 106 Wynn Drive, Huntsville, Alabama 35805
54. J. J. Dorning, Department of Nuclear Engineering and Engineering Physics, Thornton Hall, University of Virginia, Charlottesville, Virginia 22901
55. Lt Richard Engstrom, AFWL/NTCA, Air Force Weapons Laboratory, Kirtland Air Force Base, Albuquerque, New Mexico 87117
56. R. M. Haralick, Department of Electrical Engineering, University of Washington, Seattle, Washington 98195
57. Phil Jessen, Mission Research Corp., 4935 N. 30 Street, Colorado Springs, Colorado 80919
58. Claud Martin, U.S. Army Strategic Defense Command, 106 Wynn Drive, Huntsville, Alabama 35805
- 59-63. Paul Sonnenburg, Physicon, Inc., 3325 Triana Blvd., Suite A, Huntsville, Alabama 35805
64. John Tinsley, Kaman Sciences Corp., 1500 Garden of the Gods Road, Colorado Springs, Colorado 80907
65. Office of the Assistant Manager for Energy Research and Development, Department of Energy, Oak Ridge Operations, P.O. Box 2001, Oak Ridge, TN 37831
- 66-75. Office of Scientific and Technical Information, P.O. Box 62, Oak Ridge, Tennessee 37830

